PLOS COMPLEX SYSTEMS

RESEARCH ARTICLE

Geometric separability of mesoscale patterns in embedding representation and visualization of multidimensional data and complex networks

Aldo Acevedo[1], **Yue Wu**[2,3], **Fabio Lorenzo Traversa**[4], **Carlo Vittorio Cannistraci**[2,3,5]*

1 Biomedical Cybernetics Group, Biotechnology Center (BIOTEC), Center for Molecular and Cellular Bioengineering (CMCB), Technische Universität Dresden, Dresden, Germany, **2** Center for Complex Network Intelligence (CCNI), Tsinghua Laboratory of Brain and Intelligence (THBI), Tsinghua University, Beijing, China, **3** Department of Biomedical Engineering, Tsinghua University, Beijing, China, **4** MemComputing, Inc. San Diego, California, **5** Department of Computer Science, Tsinghua University, Beijing, China

* kalokagathos.agon@gmail.com

Citation: Acevedo A, Wu Y, Traversa FL, Cannistraci CV (2024) Geometric separability of mesoscale patterns in embedding representation and visualization of multidimensional data and complex networks. PLOS Complex Syst 1(2): e0000012. https://doi.org/10.1371/journal.pcsy.0000012

Editor: Aming Li, Peking University, CHINA

Received: November 3, 2023

Accepted: August 12, 2024

Published: October 3, 2024

Peer Review History: PLOS recognizes the benefits of transparency in the peer review process; therefore, we enable the publication of all of the content of peer review and author responses alongside final, published articles. The editorial history of this article is available here: https://doi.org/10.1371/journal.pcsy.0000012

Data Availability Statement: The artificial network and the synthetic data to reproduce the results of this study are provided at the GitHub repository: https://github.com/biomedical-cybernetics/

Abstract

Complexity science studies physical phenomena that cannot be explained by the mere analysis of the single units of a system but requires to account for their interactions. A feature of complexity in connected systems is the emergence of mesoscale patterns in a geometric space, such as groupings in bird flocks. These patterns are formed by groups of points that tend to separate from each other, creating mesoscale structures. When multidimensional data or complex networks are embedded in a geometric space, some mesoscale patterns can appear respectively as clusters or communities, and their geometric separability is a feature according to which the performance of an algorithm for network embedding can be evaluated. Here, we introduce a framework for the definition and measure of the geometric separability (linear and nonlinear) of mesoscale patterns by solving the travelling salesman problem (TSP), and we offer experimental evidence on embedding and visualization of multidimensional data or complex networks, which are generated artificially or are derived from real complex systems. For the first time in literature the TSP's solution is used to define a criterion of nonlinear separability of points in a geometric space, hence redefining the separability problem in terms of the travelling salesman problem is an innovation which impacts both computer science and complexity theory.

Author summary

In daily life, one may observe that birds usually move together in a coordinated fashion as flocks. However, from time to time, birds' groupings tend to appear inside the flock forming distinct mesoscale structures, which suddenly changes direction and dynamics of the flock, optimizing movements in terms of external factors such as updrafts or predators. The formation of these mesoscale patterns is fundamental for the benefit of the flock, but

travelling-salesman-path The real networks to reproduce the results of this study can be found in the following links: • Football, Karate, Polbooks, and Polblogs: http://www-personal.umich.edu/~mejn/netdata/ • Opsahl (all networks): https://toreopsahl.com/datasets/ Code Availability: The MATLAB source code to compute the community separability indices and to reproduce the results of some main figures of the study is publicly available at the GitHub repository: https://github.com/biomedical-cybernetics/travelling-salesman-path

Funding: This work was supported by the Zhou Yahui Chair Professorship award of Tsinghua University (to CVC) which paid the salary of CVC, the starting funding of the Tsinghua Laboratory of Brain and Intelligence (THBI), the National High-Level Talent Program of the Ministry of Science and Technology of China (grant number 20241710001, to CVC), and the independent research group leader running funding of the Technische Universität Dresden (to CVC). The funders had no role in study design, data collection and analysis, decision to publish, or preparation of the manuscript.

Competing interests: The authors have declared that no competing interests exist.

the individual bird is unawarely supporting the groupings formation, which emerges as a collective behavior from the birds' interaction. Formation of mesoscale patterns is ubiquitous in nature, from social to molecular scale, revealing important structural and functional properties of complex systems. Thus, techniques that analyze mesoscale patterns in data and networks are important to gain insights into the underlying system's functions. One important analysis is to map data or network information as points onto a two-dimensional plane where we can visually examine mesoscale patterns and whether their groups keep as separable as possible. Several indices can evaluate group separability, but information about intra-group diversity is neglected. In this research, a new methodology of analysis is proposed to measure group separability for mesoscale patterns while considering intra-group diversity. We propose an adaptive method for evaluation of both linearly and nonlinearly separable patterns that can evaluate how good is the representation of mapping algorithms for mesoscale patterns visualization. We found that assessing nonlinear separability benefits from solutions to the famous travelling salesman problem.

Introduction

Geometric separability of mesoscale patterns in data represented in a two-dimensional space

Measuring group separability in a geometrical space is a fundamental mission in data science and pattern recognition [1,2], because it allows assessing the extent to which algorithms for dimension reduction, embedding, and representation of multidimensional data perform well [2]. The quality of the representation can be assessed according to different criteria, and the criterion to measure the geometric group separability of mesoscale patterns evaluates the ability of an algorithm to represent at the best the mesoscale patterns hidden in the original high-dimensional data space. In this study for mesoscale patterns we intend the organization of the data samples that tend to create groups that are separated between them (*inter-group diversity*), but they retain also a meaningful internal distinction (*intra-group diversity*). And, for representing at the best the mesoscale patterns in a two-dimensional space, we intend that the groups of samples should retain both inter-group diversity and intra-group diversity. This is possible to evaluate because the group of samples are associated with some labels, which can be provided: (1) supervisedly using meta-features or meta-data designed by the users; (2) unsupervisedly by applying algorithms for data clustering, with the scope to discover new groups stratifications or to independently verify the ones expected.

In 1973, with the introduction of the Dunn index [3], the concept of cluster validity index (CVI) was presented with the aim to evaluate group separability of clusters detected in a geometric space by unsupervised algorithms for data clustering. Then, along the years, following the same philosophy, many other cluster validity indices were proposed including, to name some of the most used: in 1974 the Calinski-Harabasz index (CH) [4]; in 1979 the Davies-Bouldin index (DB) [5]; in 1987 the Silhouette index (SIL) [6]; in 1995 the Generalized Dunn Index (GDI) [7]; in 2019 the Density-involved Distance (CVDD) [8]. For more details about the mathematical formula of each of these indices please refer to the original publications because, for the reasons we explain below, they are not subject of this study.

Although not intentionally designed for that, and with the risk of inaccuracy, CVIs gained popularity in a similar applied problem, which is the one discussed in this study: on measuring the geometric group separability of mesoscale patterns in data represented in a two-dimensional space. Each of these CVIs were introduced across the decades to address different

evaluation's issues, but all of them shared the same conceptual problem. In Fig 1A we show that cluster validity indices belong to a special subclass of separability indices that enforces *compactness*, because the preservation of intra-group diversity is neglected. Indeed, as we show in Fig 1B, CH index (as any CVIs) scores higher the representation where the points of each group tend to collapse (at the limit) in one unique point (right panel of Fig 1B), favoring compactness in contrast to retain intra-group diversity (left panel of Fig 1B). CVIs favor compactness because they were designed to evaluate the performance of clustering algorithms, but this criterion is too restrictive for the evaluation of the geometric separability of mesoscale patterns in data represented in a two-dimensional space, because in this circumstance we are interested to value representations in which the intra-group diversity is preserved. Indeed, the goal of two-dimensional data representation is to explore the relative disposition of the samples inside each group and between groups.

To this aim in 1998, Thornton introduced the concept of geometric separability and an algorithm to compute the geometric separability index (GSI) [1]. The geometric separability is based on the criteria that a point should share the same label of the first-nearest neighbor in the geometric space. The GSI is defined as the proportion of data points whose classification labels are the same as those of their first-nearest neighbor. GSI can detect the presence of group separability in the presence of nonlinearity, but it cannot distinguish whether the separability is linear or nonlinear, and it seems to suffer more than the CVIs in the presence of noise or micro-cluster formations [2].

The concept of *linear separability* in a geometric space was discussed in 1969 by Minsky and Papert[9,10], who described tasks which could be handled using the Perceptron method as 'linearly separable'[1], meaning that there exists a *separability line* which segregates two groups of samples one from each other. However, a separability line was never used to design indices for evaluation of geometric separability of mesoscale patterns in data represented in a two-dimensional space. In 2022, our group in the study of Acevedo et al. [2] proposed the general data science notion termed *projection separability (PS)* [2], which contemplates diverse ways to define linear separability in respect to a *projection separability line*. The *separability line* (Fig 1B, vertical dashed black line) separates two groups of samples in a geometric space and indicates the presence of linear separability. In a 2D space, the projection separability line (Fig 1B, horizontal solid line) is orthogonal to the separability line and is used to project the samples and to assess the extent to which their organization is far from the exact linear separability in two groups. Examples of projection separability line are: (1) the projection line that connects the centroids (see example of centroid projection line in Fig 2A and 2B) of two groups of nodes in the geometric space [2], which is termed centroid projection separability (CPS); (2) the projection line defined with respect to a criterion of maximum linear data discrimination is the first component projection vector of linear discriminant analysis (LDA) [11] (see example of LDA projection line in Fig 2A and 2B), which is termed linear discriminant projection separability (LDPS)[2]. The criterion of separability for the LDPS is to maximize the ratio of the variance between groups to the variance within groups [11]. In this study we will concentrate on CPS and LDPS because they are the most efficient solutions that we have currently at hand [2], as we will motivate hereafter. In our previous study of Acevedo et al. [2], other examples and notions to define a projection line were discussed. A separability line can be obtained by any statistical or machine learning technique which maximizes a criterion of separability between two groups of data [2]. For instance, the linear binary soft margin Support Vector Machine (lbSVM)[12–14] maximizes the margin, and the line orthogonal to the maximum-margin hyperplane (the decision boundary) can be used as a projection line. Hence, the criterion of separability for the support vector projection separability (SVPS) [2] is to maximize the geometrical margin between the two groups. However, lbSVM scales cubically

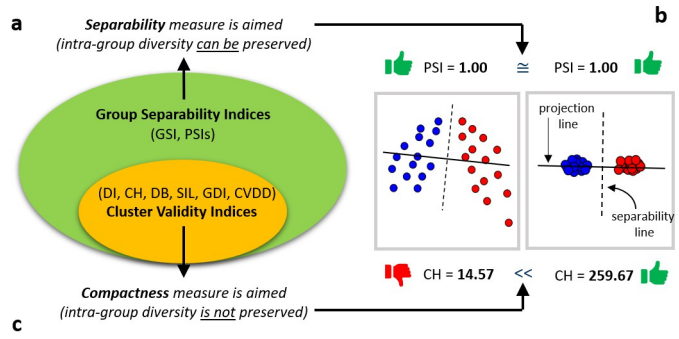

c

Index	Features		Applicability				Robustness	
	Principle	Bounded	Overlapping	Arbitrary shapes	Linear detection	Nonlinear evaluation	Isotropic noise	Anisotropic noise (outliers)
DI (Dunn, 1973)	Global comparison	✗	✗	✗	✗	✗	✗	✗
CH (Calinski et al. 1974)	Centroids	✗	✓	✗	✗	✗	✗	✗
DB (Davies et al. 1979)	Centroids	✗	✗	✗	✗	✗	✓	✓
SIL (Rousseeuw, 1987)	Global comparison	✓	✓	✗	✗	✗	✓	✗
GDI (Bezdek et al. 1995)	Global comparison	✗	✗	✗	✗	✗	✓	✓
CVDD (Hu et al. 2019)	Density	✗	✗	✓	✗	✗	✗	✗
GSI (Thornton, 1998)	Nearest Neighbor	✓	✗	✓	✗	✓	✗	✓
PSIs (Acevedo et al. 2022)	Linear Projection + statistics	✓	✓	✓	✓	✗	✓	✓

Fig 1. Group separability measures in data science: an overview. (a) Cluster validity indices are a subclass of separability measures that aim to compactness. **(b)** While group separability measures such as PSI-types aim to preserve both inter- and intra- group diversity rating the same the left and right data representations, a cluster validity measure such as CH rates higher a compact representation that neglects the intra-group diversity. This example offers evidence that using cluster validity indices for evaluation of group separability is not an appropriate solution. **(c)** Rows indicate different groups separability measures: yellow background for cluster validity measures and green for geometric separability measures. The columns indicate different *features* of the measure, their *applicability* to a spectrum of problems that arise in data science, and their *robustness* under different types of noise.

https://doi.org/10.1371/journal.pcsy.0000012.g001

with the number of samples [14,15], and its running time is in general larger than LDA. To address these time issues, Acevedo et al. [2] introduced the methodology called the centroid projection separability line (CPS), whose time complexity is O(ND) where N is the number of samples, and D is the number of dimensions. Since in our study the representation is two-dimensional, the dimension D = 2 can be considered a small constant and does not impact the time complexity. This is in general valid for any study in which the dimension D is fixed to a small constant k<<N, in which case CPS time complexity is approximated to scale linearly with the number of samples. CPS computes the geometrical centroids (median estimator) of each of the two groups, and then considers the line that connects them as a projection line (Fig 2A and 2B). CPS offers a naïve solution to measure linear separability that is more approximative than LDPS and SVPS, but the advantage in running and complexity time is remarkable in comparison to the other solutions.

Finally, a projection separability index (PSI) [2] is defined by applying any bi-class separability measure (such as the area under the curve of precision-recall, AUPR [16], or any other measure for evaluation of unbalanced data classification) directly on the projection line to

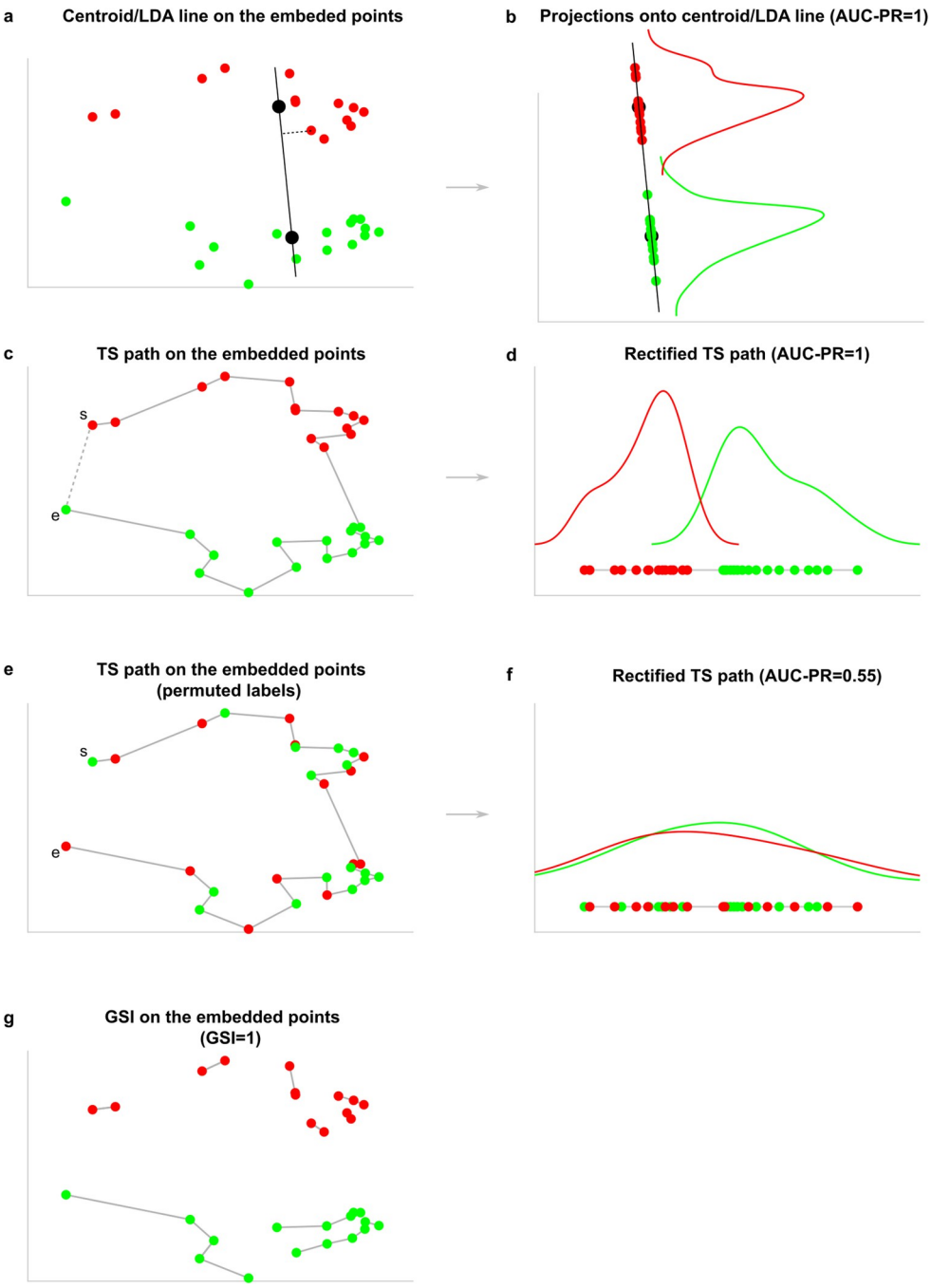

Fig 2. Geometric separability based on projection or first-neighbor strategies. (a) Example of how the centroid projection line (CPS) or the linear discriminant line (LDPS) would be drawn considering the linear geometric separability of the two community-based groups of network nodes in Fig 3C. The two black dots at the center of the plot are the centroids of the respective groups of nodes. **(b)** The nodes are projected on the projection separability line and the AUC-PR is computed to evaluate the extent of linear separability between the two groups. The AUC-PR can be substituted by any other bi-class classification measure for unbalanced data. **(c)** Travelling salesman tour (with the dashed line) and path (without the dashed line) across the points that are the nodes of the nPSO network (Fig 3) embedded in the two-dimensional space (Fig 3C). The travelling salesman (TS) path approximates the projection separability curve that accounts for the intrinsic nonlinear geometry of the data points. **(d)** The nodes are aligned on the rectified TS path and the AUC-PR is computed to evaluate the extent of separability between the two groups. **(e)** and **(f)** are respectively equivalent to (c) and (d) when the labels of the two communities are uniformly at random reshuffled to generate one instance of the null model. **(g)** The geometric separability index adopts a strategy defined as the proportion of data points whose classification labels are the same as those of their first-nearest neighbor.

https://doi.org/10.1371/journal.pcsy.0000012.g002

measure the extent to which the two groups are linearly separable. For instance, PSI was adopted with merit to evaluate the geometric linear separability of spatially organized groups of single cells embedded in a 2D and 3D space by analyzing their transcriptome [17].

GSI and PSIs values are bounded between 0 (worst result) and 1 (best result indicating data separability), while the majority of CVIs are not. Since they evaluate mere geometric separability, they are not preferentially looking for compactness as the CVIs do. For this reason, in the example of Fig 1B, PSI rates with the highest values (PSI = 1 indicates presence of linear separability) the two different patterns of separability indicating that they are both valid and of interest, whereas CH index overrates the separability pattern on the right side (CH = 259.67) because, as all cluster validity indices, aims to value compactness.

In the panel provided in Fig 1C we offer an overview of the CVIs, GSI and PSIs mentioned above together with their characteristics (see figure legend for details) considering a metanalysis based on empirical evidence conducted in the study of Acevedo et al [2]. From this comparison emerges that geometric separability-based indices, such as GSI and PSIs, perform better than cluster validity indices on many requirements, hence in this study we will consider only GSI and PSIs. GSI is the second best but it suffers in case of overlapping clusters, cannot distinguish linear from nonlinear separability and is affected by isotropic noise. PSIs are the best because they can encompass all the characteristics, but their results are affected by the presence of nonlinear separability between groups in the data. Therefore, the first aim of this study is to investigate how to extend the concept of projection separability to the nonlinear scenario.

Geometric separability of mesoscale patterns in complex networks represented in a 2D space

Complex systems are systems whose properties emerge from the interactions among their constituent parts, hence scientists in complexity science adopt networks as framework to model them. Micro-properties such as average clustering coefficient and degree probability distribution, are features of complexity that emerge from the statistical analysis of micro-structures around a network node. Yet, one of the most intriguing aspects of complexity is the capability to originate mesoscale patterns from microscopic interactions. This occurs when micro-parts of a system tend to self-organize grouping together as a result of their closer inter-playing with respect to other micro-parts.

Examples of mesoscale patterns in complex networks are: communities or modules [18], nestedness [19–21], core-periphery structures [22–24]. Formation of mesoscale patterns arises at different physical scales in natural [25] and artificial [26] complex systems: proteins create stronger interactions inside functional complexes [27]; insect swarms and bird flocks, as well as fish schools, create different internal meso-patterns with respect to external stimuli (e.g., temperature of air or water) or threats [28,29]; humans in social networks make tighter links inside communities [18]; community-layered organization can emerge during training of ultra-sparse deep learning artificial neural networks [26]. Some of these mesoscale patterns, such as in bird flocks, are directly visible because they are generated in a patent space; other patterns, such as in protein interactomes or social networks, emerge in a latent space, and the adoption of algorithms for network embedding is fundamental to visualize their presence. Visually representing mesoscale patterns helps in identifying the underlying principles of network organization and can have practical applications in various fields.

This study focuses on community organization since it emerges in many domains of applied network science. A community or module refers to a subset of nodes within a network that interact with each other more frequently than with nodes outside that specific community [18]. Communities visualization is not always straightforward. For instance, Fig 3A displays

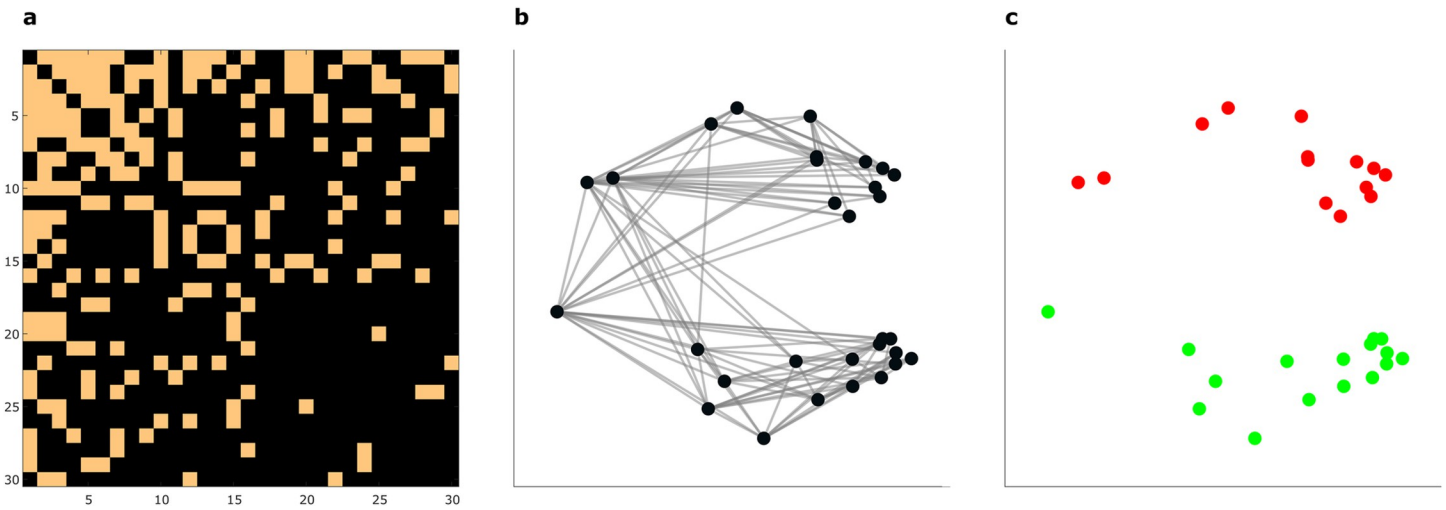

Fig 3. Geometric separability of community-based mesoscale patterns in complex networks. (a) The adjacency matrix of an artificial network with two communities generated with the nonuniform popularity similarity model (nPSO). From the adjacency matrix, the presence of any mesoscale structure associated to community organization is not visible **(b)** Embedding by the HOPE algorithm of the nPSO network in a two-dimensional geometric space reveals the presence of a geometric representation composed by two groups of nodes (one up and one down), providing evidence of network embedding efficacy to visualize the latent mesoscale structure of complex networks. **(c)** Attributing to each node a color related with the respective community type (red or green) in the network, we note that nodes in the same community locate closer to each other forming two groups in the geometric space. Evaluating the representation of a network in relation to the geometric separability of the groups of nodes formed by their communities is an innovation that we introduce in this article.

https://doi.org/10.1371/journal.pcsy.0000012.g003

the adjacency matrix associated with the unweighted network connectivity of an artificial complex network with 2 communities generated with the nPSO model [30,31]. Looking at the Fig 3A binary color visualization (orange color for observed and black color for missing interactions) of the adjacency matrix, it is not straightforward to visually distinguish the presence of mesoscale patterns that can be associated with the 2 communities in the network.

Network embedding in a geometric space of two-dimensions (2D) [32,33] plays a crucial role in the visual representation, discovery, investigation and interpretation of mesoscale patterns hidden in the structure of a complex network. When Fig 3A adjacency matrix is represented by a network embedding algorithm (in this case, HOPE [34]) in a 2D geometric space (Fig 3B), we can visually recognize the presence of the 2 communities (compare their pattern with their ground truth node's colors in Fig 3C) showing the utility of network embedding to discover patterns in complex data analysis [35–38]. Yet, new challenges [39] emerge after the data embedding. For instance, how close or far, how similar or distant are these mesoscale structures which are associated to communities in the networks? The calculation of the separability of the communities in the two-dimensional geometric space can be used for instance: (1) to evaluate the performance of network embedding algorithms or to guide the best tuning of their hyperparameters; (2) to evaluate the similarity between the mesoscale organization of diverse complex networks according to the geometric separability of their communities. In the first case, the more the algorithms clearly disclose and display the community structure of the networks in the two-dimensional space, the better their performance is rated. In the second case, the closer is the evaluation of community geometric separability between networks that are generated from the same complex system, the higher is their similarity in their mesoscale organization.

Hence, we introduce and test also in network science the notion of linear and nonlinear geometric separability of mesoscale patterns [1,2] which, in the specific case of this study,

concerns measuring the geometric separability of the groups of network's nodes that form the communities.

Results

Innovations of this study

The first innovation of this study is to offer a general definition of *projection separability (PS)* for points in a geometric space which include also the notion of projection separability curve (PSC) to address nonlinear separability problems. We propose that to assess the geometric separability of two generic sets of points that form mesoscale patterns in a representation space, a measure of projection separability projects or connects the points by ordering them on a line (linear separability, Fig 2A) or a curve (nonlinear separability, Fig 2C) in relation to their geometric proximity in the representation space. The projection separability line/curve represents a 1D projection of the bi-class points that is meaningful (according to a certain discrimination criterion) for their separation in two classes. Once the nodes are projected on a line or curve, a projection separability index (PSI) is defined by applying any bi-class separability measure (such as the area under the curve of precision-recall, AUPR [16], or any other measure for evaluation of unbalanced data classification) directly on the projection line (Fig 2B) or rectified curve (Fig 2D) to measure the extent to which the two groups are separable. For data with a multi-group structure, the average PSI among all pairs of groups is considered as an overall measure. This means that the performance of a PS measure is always between 0 (worst result) and 1 (best result). Note the previous definition of projection separability (PS) provided by Acevedo et al [2]. was limited to the case of linear separability (Fig 2A and 2B) evaluated by the projection separability line, which is a sub-case of projection separability curve. In contrast, the geometric separability index proposed by Thornton (GSI)[1] - that is based on the criterion of nearest neighbor label-similarity–offers a solution (Fig 2E) which does not order the points according to their proximity on a curve, hence it cannot be used for projection separability. The example in Fig 2A, 2B, 2C and 2D shows that in case of a linear separability problem where the two groups (red and green dots, Fig 2A) are linearly separable in the geometrical space, in principle, both a projection separability line (Fig 2A and 2B) and a projection separability curve (Fig 2C and 2D) are able to offer an appropriate quantification of perfect linear separability (AUC-PR = 1, Fig 2B and 2D). However, in this study we extend our investigation to the case of nonlinear separability problems such as in Figs 5F–5I and 6F–6N, which we will discuss in the next section *Empirical evidence on artificial datasets*. At this stage, after having introduced the notion of projection separability curve (PSC), a problem arises on how to estimate it.

The second innovation is on the methodology to compute a projection separability curve, for which we need to select a criterion of nonlinear separability and optimize it. We propose to approximate the projection separability curve by solving the travelling salesman problem (TSP) via a very efficient TSP solver such as Concorde [40]. The solution of the TSP is a tour (see example in Fig 2C) from which, by removing the connection of maximum length (dashed connection in Fig 2C) between the two groups, we extract the path of minimum length that travels across all the data points or network nodes embedded in a geometric space. We define this type of nonlinear projection separability as travelling salesman projection separability (TSPS) and the associated projection separability curve as travelling salesman projection separability curve (TS-PSC). Therefore, in this study we arrive at a complete and general definition of the projection separability of data or network nodes in a geometrical space by using a projection separability line (computed as CPS or LDPS, see previous study of Acevedo et al. [2]) or using a projection separability curve (computed as TSPS). The projection separability curve

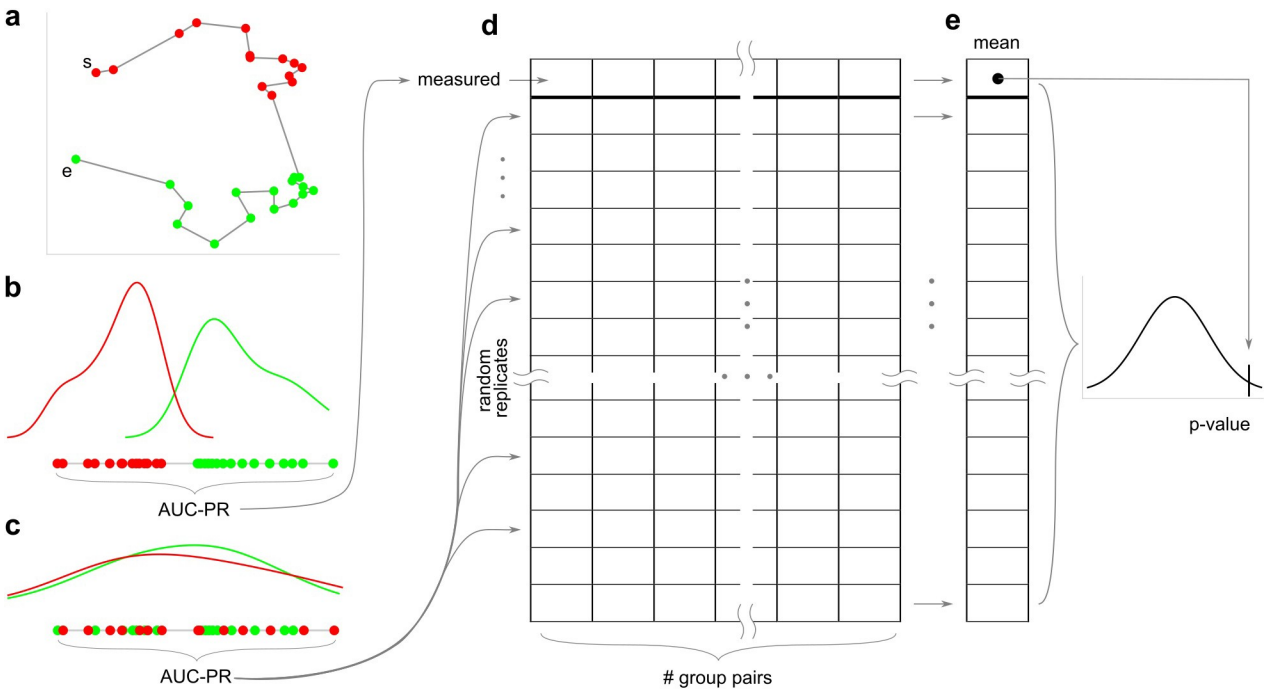

Fig 4. Statistical significance of the travelling salesman projection separability (TSPS) measure. (a) The travelling salesman (TS) path that connects the points to be rectified **(b)** and the AUC-PR is computed for assessing the separability of the observed group organization embedded in the geometric space. **(c)** the labels of the groups are uniformly at random reshuffled and the AUC-PR is computed to generate a random instance. **(d)** the process to generate random replicates is repeated for a certain number of times (rows, n = 1000 in our study) and for all number of group pairs (columns). **(e)** Then the mean value across the group pairs (columns) is computed to generate the final value to build a null model distribution. The p-value of the observed TSPS measure is computed as the fraction of random values that are larger than the observed value.

https://doi.org/10.1371/journal.pcsy.0000012.g004

is proposed to help in the case of data spatially organized according to a nonlinear separability problem. As introduced for projection separability line in the previous study of Acevedo et al. [2], also here in the case of projection separability curve we can compute an empirical p-value that expresses the extent to which the PSI measure is statistically significant. Henceforth we visually explain the main steps of the procedure, and the technical details are provided in the Method section. Keeping fixed the solution of the TS-PSC, the ground-truth-group labels (Fig 2C) are shuffled uniformly at random (Fig 2E) and the AUC-PR is computed on the rectified curve (Fig 2F). This process (Fig 4A, 4B, 4C) is repeated several times to create a fixed number m (in this study $m = 1000$ realizations, see Method section) of random replicates AUC-PR estimations (Fig 4D, m rows of the matrix) for each pair of groups in the data (Fig 4D, columns of the matrix). Then, to build a null model the mean replicate values across the different group pairs (across the columns) is computed and the mean values are used to build a null model distribution (Fig 4E). The empirical p-value is computed considering the proportion (in respect to all the values m+1: m random values and 1 true measured value) of randomly-generated values that are larger than true-measured (observed) value.

The third innovation is to introduce in network science the concept of projection separability of the community's nodes of a complex network represented in a geometric space (community projection separability, CoPS). For a network whose nodes lie or are embedded in a geometric space, in order to assess the geometric separability of nodes across two communities, we can project or connect their nodes on a projection separability line or curve. According to this definition of coPS we can compute any projection separability index (PSI), which is calculated by applying any bi-class separability measure (such AUC-PR [16]) directly on the

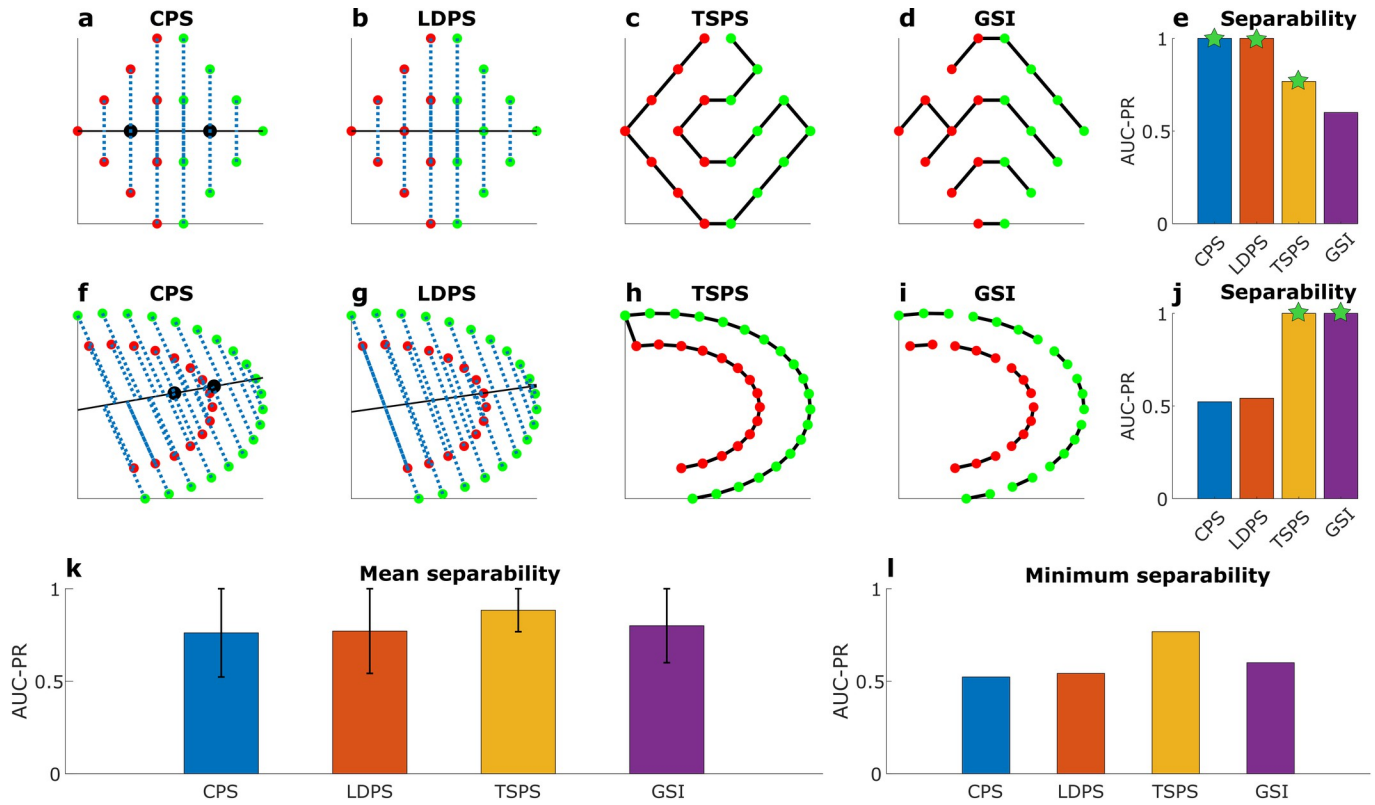

Fig 5. Linear and nonlinear separability in complex data science. Red and green dots indicate the samples of two different groups. (a-e) refer to an example of a linearly separable dataset called Rhombus. (f-j) refer to an example of a nonlinearly separable dataset called Halfkernel. **(a, f)** centroid projection separability (CPS): the two black dots indicate the centroids (median estimator) of the two groups of samples, the black line indicates the projection line, the vertical blue dashed lines indicate the projections of the samples. **(b, g)** linear discriminant projection separability (LDPS): the black line indicates the first component projection vector of the linear discriminant analysis (LDA), the other graphics are as for (a). **(c, h)** Travelling salesman projection separability (TSPS): the travelling salesman path across the samples is indicated by the black solid lines. **(d, i)** geometrical separability index (GSI): the black solid lines indicate the first neighbor sample matching. **(e, j)** separability of each measure in the respective dataset: (e) Rhomboid and (j) Halfkernel. **(k, l)** mean and minimum separability of each measure across the two datasets. In **(e, j)** the values of the indices with a significant (p-value < 0.01) geometric separability are marked with a star, which means that these values are very unlikely to be obtained by chance.

https://doi.org/10.1371/journal.pcsy.0000012.g005

projection line (Fig 2B) or rectified curve (Fig 2D) to measure the extent to which the two communities of network's nodes are separable. For networks with a multi-community structure, the average PSI among all pairs of communities is considered as an overall measure of community separability. This means that the performance of a PS measure is always between 0 (worst result) and 1 (best result). Note that there exist many criteria to define the separability of community directly from the network structure, such as modularity [41], and they are used to implement community detection algorithms. However, here our innovation is to propose a criterion to evaluate the representation of a network in a geometric space with respect to the quality of representation of its mesoscale community structure. And, for representing at the best the mesoscale community structure in a two-dimensional space, we intend that the nodes should preserve in the geometric space both inter-community diversity and intra-community diversity. In addition, for each PSI evaluation on the community projection separability, an empirical p-value that expresses the statistical significance of PSI evaluation is computed according to the procedure described above in this section.

The fourth innovation of this study is in multidimensional analysis of the network community organization. The analysis is multidimensional because we consider the effect of many

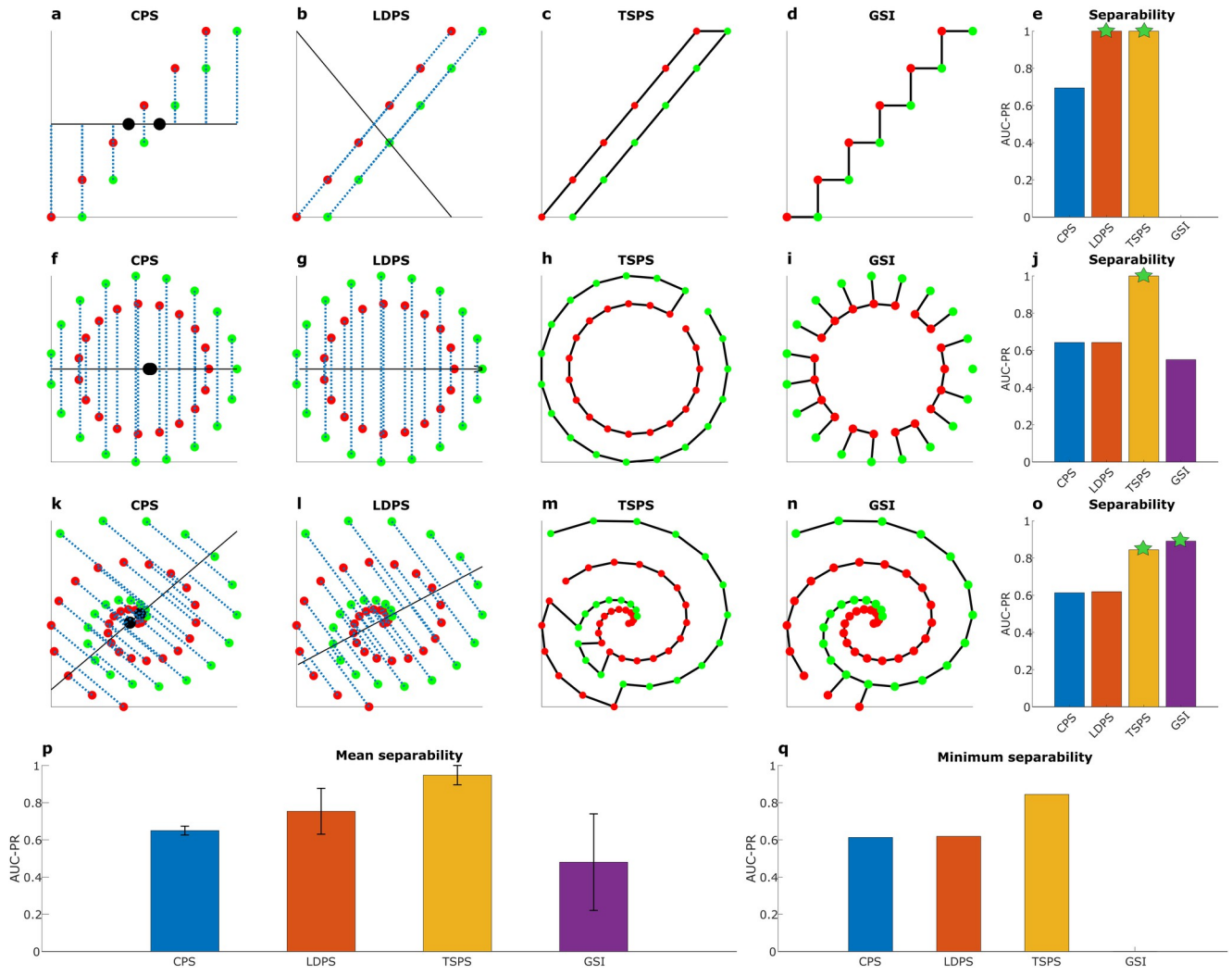

Fig 6. Hard separability problems in complex data science. Examples of hard separability problems, the term 'hard' indicates difficulty to detect the presence of separability. (a-e) refer to an example of a linearly separable dataset called Parallel lines. (f-j) refer to an example of a nonlinearly separable dataset called Circles. (k-o) refer to an example of a nonlinearly separable dataset called Spirals. **(a, f, k)** Centroid projection separability (CPS): the two black dots indicate the centroids (median estimator) of the two groups of samples, the black line indicates the projection line, the vertical blue dashed lines indicate the projections of the samples. **(b, g, l)** Linear discriminant projection separability (LDPS): the black line indicates the first component projection vector of the linear discriminant analysis (LDA), the other graphics are as for (a). **(c, h, m)** Travelling salesman projection separability (TSPS): the travelling salesman path across the samples is indicated by the black solid lines. **(d, i, n)** Geometrical separability index (GSI): the black solid lines indicate the first neighbor sample matching. **(e, j, o)** separability of each measure in the respective dataset: (e) Parallel lines, (j) Circles and (o) Spirals. **(p, q)** mean and minimum separability of each measure across the three datasets. In **(e, j, o)** the values of the indices with a significant (p-value < 0.01) geometric separability are marked with a star, which means that these values are very unlikely to be obtained by chance.

https://doi.org/10.1371/journal.pcsy.0000012.g006

features together in contrast to unidimensional analysis where the effect of each feature is considered alone and independently from the others. We propose a multivariate analysis that we name multivariate community separability analysis (MCSA), which adopts principal component analysis (PCA) to represent in a 2D space two different scenarios: (i) the first scenario, that we call multivariate community separability analysis of the methods' performances (MCSAmp), considers how similar are the performances of the embedding methods evaluated using different community projection separability measures in respect to features which are the values of community projection separability across different networks; (ii) the second scenario, that we call multivariate community separability analysis of the network representations

(MCSAnr), considers how similar are the network representations obtained using different embeddings in respect to features which are the values of community projection separability across different measures. In the section below *Empirical evidence on real network*, we will discuss the applications of MCSA on real data from network science.

Empirical evidence on artificial datasets and the adaptive geometrical separability (AGS)

Fig 5 showcases performance of geometric separability measures when they are tested on artificial datasets with linear and nonlinear separability problems in complex data science. Fig 5E shows that CPS and LDPS perform better than TSPS and GSI in the provided linear separability problem (Fig 5A–5D), offering evidence that, when a problem is linearly separable, their performance (estimated using the area under the precision-recall curve, AUPR) might overcome the one of nonlinear methods. Note that the geometric separability estimated by GSI is the only not statistically significant (Fig 5E, green stars indicate statistical significance with p-value$<$0.01). Conversely, Fig 5J shows that CPS and LDPS perform worse than TSPS and GSI in the provided nonlinear separability problem (Fig 5A–5D), offering evidence that, when a problem is nonlinearly separable, the nonlinear methods can overcome the linear ones. Note that the geometric separability estimated by CPS and LDPS are not statistically significant (Fig 5J, green stars indicate statistical significance with p-value$<$0.01). When we take the mean performance (Fig 5K) of these methods across the two problems, TSPS performs the best, meaning that TSPS is the most versatile method. Besides, when we take the minimum performance (Fig 5I) across the two problems, TSPS performs again the best meaning that it is the most robust method. The stars in Fig 5E and 5J indicate that TSPS is the only measure statistically significant in both cases, indicating that TSPS produces estimations which can be reliable regardless of the linear or nonlinear origin of the problem.

Fig 6 displays the performance of the same methods on three different examples of hard separability problems, where the term 'hard' in this context means difficulty to detect the presence of separability. The first example (Fig 6A–6D) presents the difficulty of two groups that are linearly separable but are very close to each other. Fig 6E provides a bar plot that compares the results of the different separability measures. In this scenario: CSP (Fig 6A) suffers from bad performance because it detects a wrong linear separability line; GSI (Fig 6D) suffers from null performance because it matches pairs of samples of the opposite classes; LDPS (Fig 6B) and TSPS (Fig 6C) offer the perfect solution. LDPS and TSPS only are statistically significant (Fig 6E, green stars indicate statistical significance with p-value$<$0.01). The second example (Fig 6F–6I) present the difficulty of two groups that are nonlinearly separable because they are concentric circles with different radius. Fig 6J provides a bar plot that compares the results of the different methods. In this scenario: CSP and LDPS (Fig 6F and 6G) suffer from the same bad performance because they detect the same linear separability line that does not assess the correct separability, indeed this is a nonlinear problem, hence it is by definition linearly unsolvable; GSI (Fig 6I) also suffers from bad performance because it occasionally matches pairs of samples of the opposite class; TSPS (Fig 6H) offers the perfect solution which is also statistically significant (Fig 6J, green stars indicate statistical significance with p-value$<$0.01). The third example (Fig 6K–6N) presents the difficulty of two groups that are nonlinearly separable because they are following two concentric spirals of different radius. Fig 6O provides a bar plot that compares the results of the different methods. In this scenario: CSP and LDPS (Fig 6K and 6I) suffer from bad performances because they detect two different linear separability lines that do not assess the correct separability, indeed this is a nonlinear problem, hence it is by definition linearly unsolvable; GSI (Fig 6N) offers the best but still not the perfect

solution; TSPS (Fig 6M) offers the second best result because the solution to the TSP provided by Concorde algorithm suffers of few jumps that result in wrong connections across the two different groups. TSPS and GSI only are statistically significant (Fig 6O, green stars indicate statistical significance with p-value<0.01). When we take the mean performance (Fig 6P) of these methods across the three problems, TSPS performs the best, meaning that TSPS is the most versatile method. Besides, when we take the minimum performance (Fig 6Q) across the three problems, TSPS performs again the best, meaning that is the most robust method. The stars in Fig 5E, 5J and 5O indicate that TSPS is the only measure statistically significant in the three cases, indicating that TSPS produces estimations which can be reliable regardless of the 'hardness' of the problem.

Results on these artificial datasets show that TSPS is the most versatile and robust of the four tested measures for separability estimation; however, different measures can magnify their performance in relation to the different types of separability problems. Therefore, we propose an adaptive geometrical separability (AGS) estimation that, for each type of dataset (or network), can assess the extent to which the groups in the data (or communities in networks) present linear or nonlinear empirical separability, and can identify the best solver (i.e., measure) to achieve such maximal separability performance.

Empirical evidence on real complex multidimensional data

Fig 7 reports results on the radar signal dataset [42], which is a benchmark for testing the ability of embedding techniques to solve the crowding problem [43], which means that after two-dimensional embedding, the different groups of samples tend to collapse on top of each other (highly overlapping) in the representation space. Hence, evaluating the correct group separability is challenging and the complexity of this dataset is associated with the mix of hierarchical and similarity relations between the data samples (radar signals) in a multidimensional feature space. Indeed, the radar signal dataset is composed good radar signals that are highly similar, and bad radar signals that are highly dissimilar. It counts 350 valid samples, 34 features, and three groups: good radar signal, bad radar signal type1 and bad radar signal type2. We

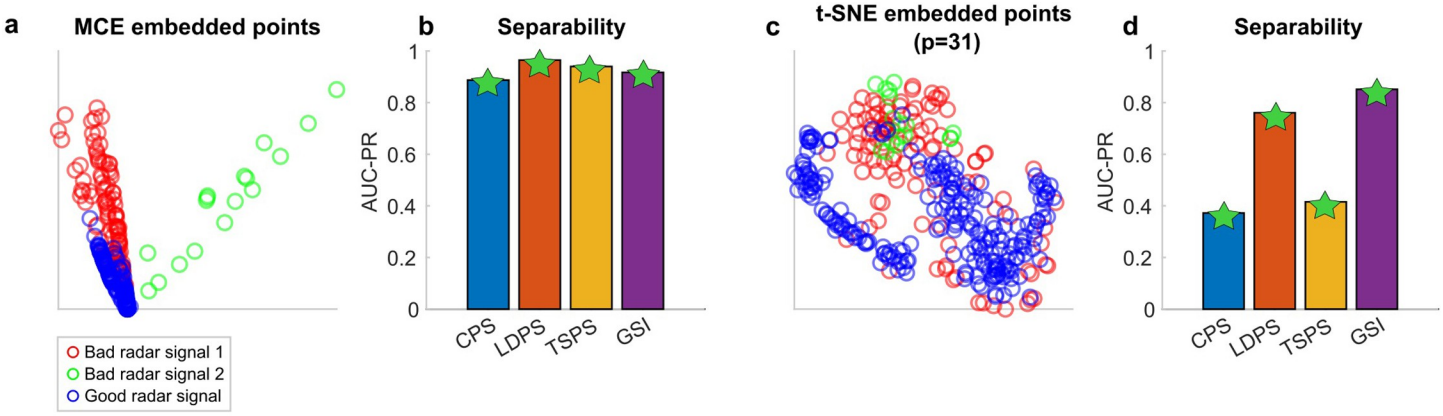

Fig 7. ***Empirical evidence on real complex multidimensional data.*** The radar signal dataset is composed of 350 valid samples, 34 features, and three groups: good radar signal, bad radar signal type1 and bad radar signal type2. The complexity of this dataset is associated with the mix of hierarchical and similarity relations between the data samples. **(a)** Embedding of the radar signal dataset in the two-dimensional space by MCE algorithm. **(b)** The geometric separability of MCE representation is estimated of high quality (performance larger than 0.8) according to any type of measure, because MCE algorithm is able to produce a representation that accounts for hierarchical structure in the data. **(c)** t-SNE representation (p = 31 is the best perplexity setting, see text for details) suffers from the crowding problem because t-SNE algorithm does not well preserve hierarchical organization. **(d)** the geometric separability measures confirm that the representation of t-SNE is of less quality of MCE for what concerns the separability of the data group structure in the representation space. In **(b,d)** the values of the indices with a significant (p-value < 0.01) geometric separability are marked with a star, which means that these values are very unlikely to be obtained by chance.

https://doi.org/10.1371/journal.pcsy.0000012.g007

performed the embedding in the two-dimensional space considering two baseline methods, and we specifically selected them since they are based on different and complementary principles of embedding. Minimum Curvilinear Embedding (MCE) [32] is an approach for data embedding that leverages the hierarchic topological information of the data and it is parameter-free, hence offering a unique solution. t-Distributed Stochastic Neighbor Embedding (t-SNE)[44] minimizes the Kullback-Leibler divergence between the joint probabilities of the low-dimensional embedding and the high-dimensional data, it presents the hyperparameter perplexity (p), which is a smooth measure of the effective number of neighbors and accounts for the balance between local and global aspects of the data. In our tests the perplexity p of t-SNE was fixed to the value that offered the best average performance across the tested geometric separability measures.

MCE is able to address quite well the crowding problem which displays an intrinsic hierarchical mesoscale structure of the radar signal dataset (Fig 7A), therefore all the four tested geometric separability measures perform similarly well (Fig 7B), offering statistically significant results (Fig 7B). t-SNE is based on an embedding strategy that suffers more for data with highly intrinsic hierarchical mesoscale structure, indeed the representation in the two-dimensional space is more crowded (Fig 7C). This results in the performance of the geometric separability measures being all statistically significant but not homogenous: LDPS and GSI indicate higher separability than CPS and TSPS. However, according to the adaptive geometrical separability (AGS) strategy we should select as final estimation the highest, which is provided by GSI. GSI's value on this t-SNE representation is in the same range but lower than the values of geometric separability on the MCE representation, indicating that MCE works better than t-SNE for representing the intrinsic mesoscale structure of the multidimensional data. This example helps to understand how to evaluate the quality of embedding and visual representation of real complex multidimensional data considering the geometric separability measure of their mesoscale group structure.

Empirical evidence on real complex networks

In this section, we report the results of applying our methodology to eight real social networks with different community organizations. The Zachary's Karate Club represents the friendship between the members of a university karate club in the United States (US). Its two communities are formed by splitting the club into two parts, each following one different trainer. The four Opsahl networks are intra-organizational networks: Opsahl_8 (7 communities), Opsahl_9 (7 communities), Opsahl_10 (4 communities), and Opsahl_11 (4 communities). The Polbooks network represents frequent co-purchases of books concerning US politics on *amazon.com*. Its three communities are associated with the political orientation of the books as either conservative, neutral or liberal. The Football network presents games between colleges during the regular season in the fall of 2000. Its 12 communities are the conferences that each team belongs to. The Polblogs network consists of links between blogs about the politics in the 2004 US presidential election. Its two communities represent the political opinions of the blogs (right/conservative and left/liberal). More details about these network datasets are provided in the methods section.

Furthermore, we investigate the performance of three baseline methods for network embedding: HOPE [34] has one hyperparameter to tune that we set to the default value, because according to some preliminary tests we found it does not substantially change the embedding in a way that is relevant for this study; ProNE [45], which does not have hyperparameters to tune and also provides a sparse matrix factorization version called ProNE (SMF); and Node2vec [46], which has two hyperparameters to tune (return parameter p and inOut

parameter q) that we fine-tuned to select the best performance, because according to some preliminary tests we noted they substantially change the embedding in a way that is relevant for this study. The rationale behind selecting these three embedding methods lies in their diverse computational strategies, which provide a wide spectrum of potential results for testing in our study. HOPE (High-Order Proximity Preserving Embedding) is a matrix-factorization-based technique that preserves high-order proximities within networks. It captures the symmetric transitivity present in large-scale graphs. ProNE (Proximity Network Embedding) is a sparse matrix factorization method specifically designed to address scalability challenges in complex and large networks, retaining localized and global clustering network information. Node2vec is a skip-gram-based approach that focuses on generating feature representations that maximize the likelihood of preserving network neighborhoods in a reduced-dimensional space. It achieves this by employing a second-order random walk strategy. More details about these embedding algorithms are provided in the methods section.

Fig 8A and 8B display the same representation edited according to different graphic settings, and they report the result of the multivariate community separability analysis of the methods' performances (MCSAmp). Each data point indicates the performance of an embedding method according to a certain community separability measure evaluated in the multidimensional space of the eight networks and embedded by PCA in a two-dimensional space of

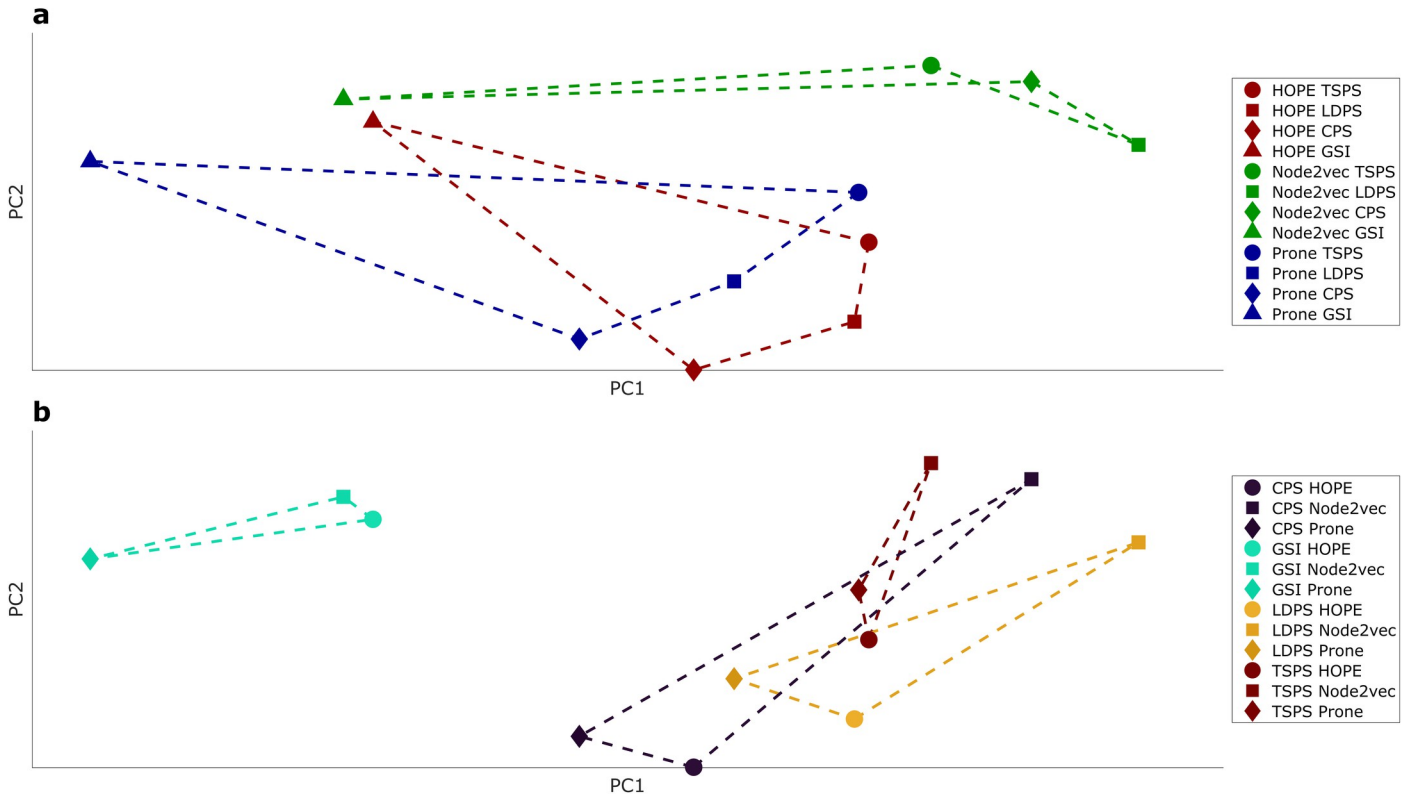

Fig 8. The multivariate community separability analysis of the methods performances (MCSAmp). x-axis for PC1 and y-axis for PC2. **(a)** spots of the same shape represent the same separability measure, spots of the same color represent the same embedding method, the dashed lines of the same color connect the same embedding method evaluated using different separability measures across the networks. Node2vec (green polygon) produces network representations that do not overlap with the ones of other methods. **(b)** spots of the same shape represent the same embedding method, spots of the same color represent the same separability measure, the dashed lines of the same color connect the same separability measure evaluated on the representations of different embedding methods across the networks. GSI (green triangle) produces separability evaluations that do not overlap with the ones of other measures.

https://doi.org/10.1371/journal.pcsy.0000012.g008

principal components one and two (PC1 and PC2, respectively). Fig 8A is created by connecting the data points that indicate the same type of embedding method: the polygon (green) formed by Node2vec performances is far from the ones of ProNE and HOPE that are overlapping. This result indicates that ProNE and HOPE have a similar embedding performance that differs from Node2vec. Fig 8B is created by connecting the data points that indicate the same type of community separability measure: the triangle (green) formed by GSI evaluations is far from the overlapping ones of CPS, LDPS, and TSPS. This result indicates that CPS, LDPS and TSPS have a similar evaluation trend that differs from GSI, which can be explained by their common projection separability nature. The triangle (brown) formed by TSPS is smaller than the triangles formed by the other projection separability measures; this means that TSP produces evaluations that are closer to each other and, therefore, more consistent across different embedding methods than the other projection separability measures.

Fig 9A reports the result of the multivariate community separability analysis of the network representations (MCSAnr). Each data point indicates the community separability of a specific network according to an embedding method evaluated in the multidimensional space of the 4 community separability measures and embedded by PCA in a two-dimensional space of principal components one and two (PC1 and PC2, respectively). The data points that indicate the same type of network are connected. The two triangles formed by Football and Karate are at opposite sides of the PC1 axis, indicating that these networks largely differ in the level of community separability. Indeed, Fig 9B reports the adaptive geometric separability (AGS) level for each embedding method in each network, and precisely, Football's AGS levels are lower than the Karate ones. This is visually evident in Fig 10, where the 2D embeddings of Football according to Node2vec (Fig 10A), HOPE (Fig 10B) and ProNE (Fig 10C) display a lower separability of the 12 communities with respect to the 2D embeddings of Karate, for which the separability of the 2 communities is perfect (value 1) in case of Node2vec (Fig 10G) and HOPE (Fig 10H), and almost perfect (value 0.997) for ProNE (Fig 10I). Besides, all these results reported a significant geometric separability (p-value$<$0.01). The two triangles formed respectively by Karate and Polblogs are on the same side (right) of the PC1 axis, indicating that these networks should have a comparable level of community separability, although for Polblogs it should be slightly lower because Karate has the highest PC1 coordinate. Indeed, in Fig 9B, Karate's AGS levels are comparable with Polblogs ones but slightly higher. This is visually confirmed in Fig 10, where the 2D embeddings of Polblogs according to Node2Vec (Fig 10D), HOPE (Fig 10E) and ProNE (Fig 10F) display a lower separability of the 2 communities with respect to the 2D embeddings of Karate (Fig 10G–10I), for which the separability of the 2 communities is perfect or almost perfect. The four triangles of the respective 4 Opsahl networks are partially overlapping at the center of the figure, indicating that they have comparable levels of community separability, which is confirmed in Fig 9B observing at their AGS levels. From Fig 9C, which reports the minimum and mean AGS of each embedding method across the networks, Node2vec emerges as the most versatile and robust method, offering the 2D representation with the highest community separability across the investigated methods. However, Node2vec has two hyperparameters to fine-tune; therefore, it makes sense that it has larger versatility and wider margin to improve performance than HOPE and ProNE.

Discussion

We provide a framework for the definition and measure of the linear and nonlinear geometric separability of mesoscale patterns in 2D visualization of complex data and networks. We adopt two linear measures and two nonlinear measures. One of these nonlinear measures is proposed in this study, and it is based on solving the travelling salesman problem (TSP). Then, we focus

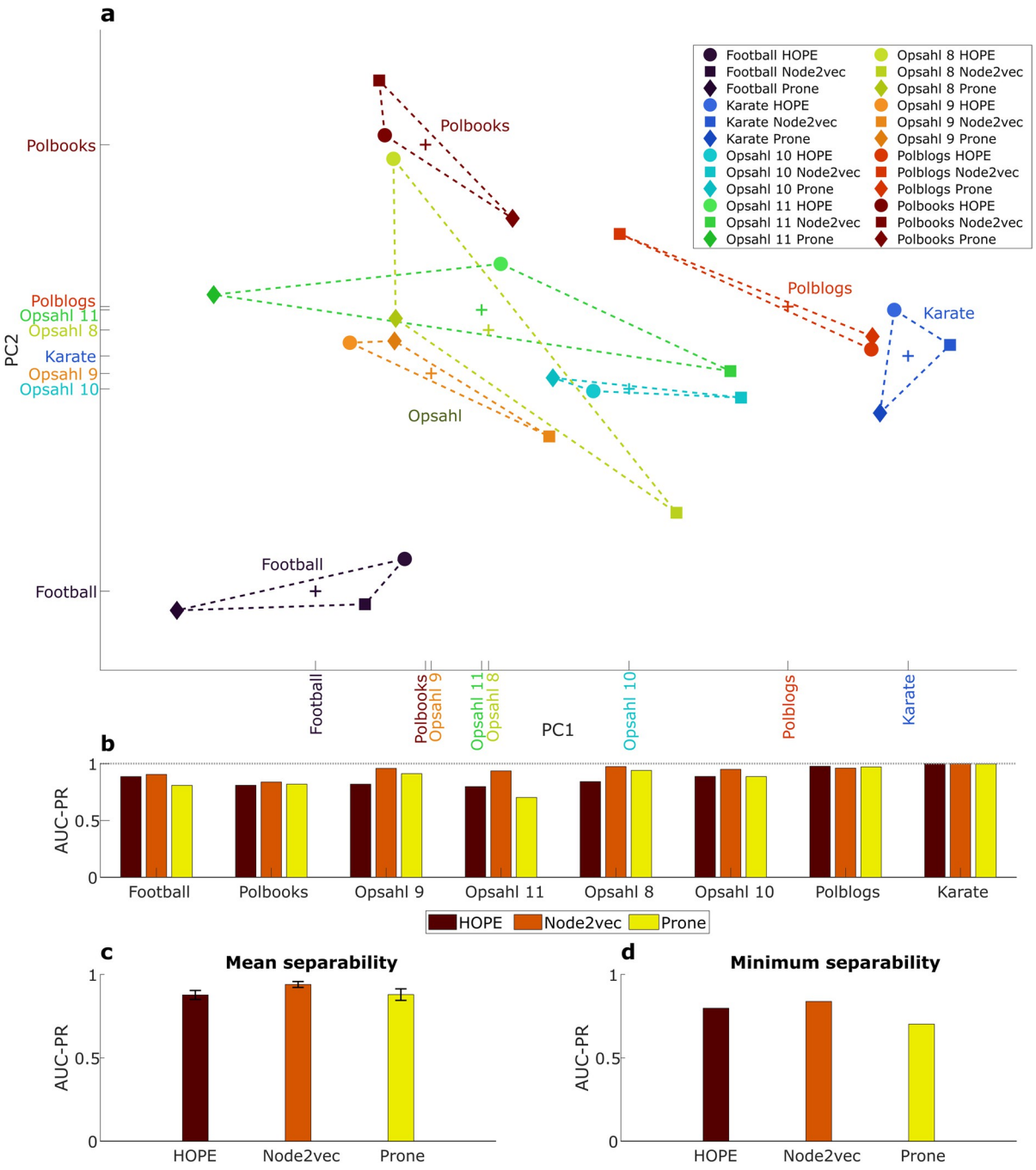

Fig 9. The multivariate community separability analysis of the network representations (MCSAnr). x-axis for PC1 and y-axis for PC2. **(a)** spots of the same shape represent the same embedding method, spots of the same color represent the same network representation, the dashed lines of the same color connect the same network's representations evaluated using different separability measures across the networks. **(b)** adaptive geometric separability (AGS) values evaluated in each network for the three different embedding methods. **(c)** mean separability of each embedding method across the networks. **(d)** minimum separability of each embedding method across the networks.

https://doi.org/10.1371/journal.pcsy.0000012.g009

on applications, investigating both real complex multidimensional data and real networks visual representations in a two-dimensional space. We measure the extent to which the embedding of data or networks in a two-dimensional space can produce a representation that unfolds

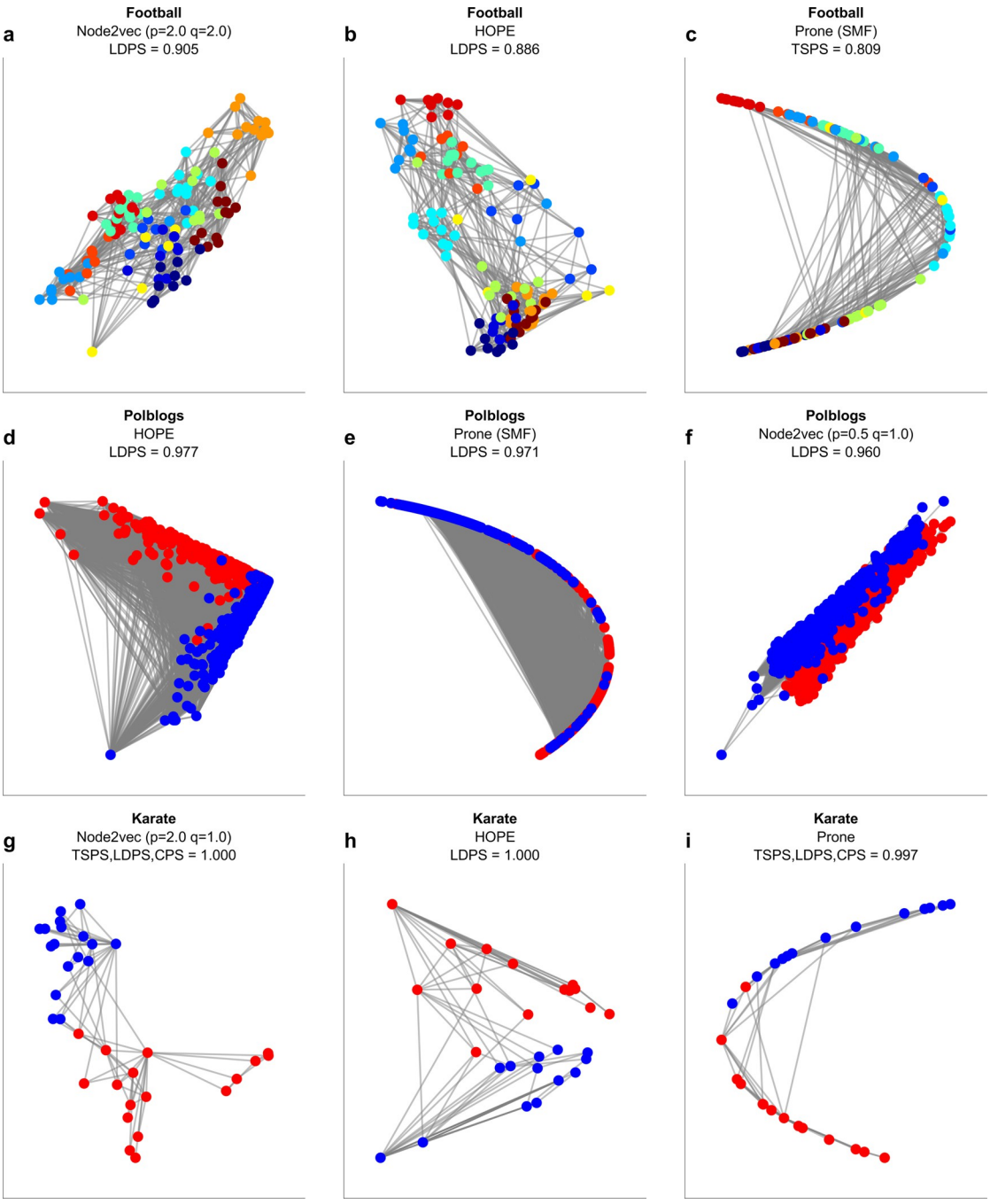

Fig 10. Two-dimensional representations of Football, Polblogs and Karate according to the different embedding methods. x-axis for the first dimension of embedding and y-axis for the second dimension of embedding. The name of the represented network is reported in bold on top of each panel, the name and hyperparameter settings (when available) of the network embedding method are reported under the network name, the adaptive geometric separability (AGS) value together with the name of the separability measure/s that achieved the maximum is reported under the embedding method name.

https://doi.org/10.1371/journal.pcsy.0000012.g010

its mesoscale structure, which means to represent distinguishable group in multidimensional data or communities in networks. Yet, without loss of generality, the tools we propose can be applied to measure group separability in a geometrical space of any dimensionality.

In our previous study [2] we introduced a methodology to measure linear separability based on a projection separability line, in this study we extend this methodology to measure also nonlinear geometric separability introducing as innovation the projection separability curve. We propose to approximate the projection separability curve by solving the travelling salesman problem (TSP) via a very efficient TSP solver such as Concorde [40] algorithm. The solution of the TSP is a tour from which is obtained the path of minimum length that separates the groups/communities travelling across all the data points or network nodes embedded in a geometric space. We define this type of nonlinear projection separability as travelling salesman projection separability (TSPS). We stress this is the first time in literature that the TSP is employed to define a criterion of nonlinear separability of data in a geometric space, hence the idea to redefine a problem of nonlinear geometric separability as a specific case of the travelling salesman problem is an innovation both in computer science and complex data analysis.

Results on artificial and real multidimensional datasets show in which scenarios TSPS is the only method offering a fair assessment of nonlinear geometrical data separability. In contrast, we comment on other cases in which mere linear projection separability is more appropriate. Therefore, we propose an adaptive geometric separability (AGS) method that, for each type of dataset (or network), can assess the extent to which the group (or community) separability is linear or nonlinear, and what is the best solver to achieve such geometrical group separation.

The motivation to investigate real applications in network embedding is that this field has been developing as a vibrant research topic in recent years [34,35,45,46], and the study of appropriate ways to evaluate its performance is currently on the verge [47]. The most employed strategies are task-oriented evaluations applied to the network or its node embedded in the geometric space, for instance: link prediction [48], geometric-weighted network community detection [35], node clustering, etc. [49,50]. These approaches rely on applying unsupervised algorithms whose performance in a specific task is considered a reference to assess the quality of the network embedding. Differently from these past methodologies, in this study we diverge from a task-oriented evaluation of embedding, and we propose to evaluate the ability of an algorithm to preserve the mesoscale organization of a network, which means to offer a 2D representation that discloses and clearly depicts the community organization. Hence, one of our innovations is to introduce in network science the adoption of a criterion that distinguishes between linear and nonlinear separability of communities in a geometric space to evaluate the network representation.

The final innovation of this study is to propose a multivariate analysis that we name multivariate community separability analysis (MCSA), which adopts principal component analysis (PCA) to represent in a 2D space two different scenarios: (i) how similar are the performances of embedding methods evaluated using different community projection separability measures in respect to the values of community projection separability across different networks; (ii) how similar are the network representations obtained using different embeddings in respect to the values of community projection separability across different measures. We test and validate these multivariate community separability analyses on real networks, discovering similarities between embedding methods, analogies between separability measures, and affinities between networks' mesoscale structures.

Altogether, these innovations pave the way toward defining quantitative tools for analyzing the linear and nonlinear separability of mesoscale patterns in complexity science and pattern recognition.

Some limitations to consider for investigation in future studies are discussed hereafter. Although Concorde [40] algorithm is a very efficient TSP solver, the computation of large datasets with hundred thousand of points can be time consuming. Hence the definition of new efficient criteria to approximate the projection separability curve should be considered as an

interesting direction of research. For instance, solutions provided by greedy algorithms such as the minimum spanning tree cold be compared with the TSP. This study is focused on evaluation of geometric group separability in a two-dimensional visual representation space, however the same methods (without necessity of any formal adjustment) could be used in the future to investigate geometric separability in higher dimensional space.

The possible implications and applications of our research on geometric separability of network community in various fields, such as biological networks, transportation systems, and more is straightforward. For instance, we could apply the multivariate community separability analysis (MCSA), to evaluate how different are the brain MRI structural connectome representations of control and unhealthy subjects considering the mesoscale lobular brain organization, which has been proven to be reflected in the brain connectome topology and geometry [51,52]. Or to evaluate the geometric separability of gene communities in co-expression networks across different tissues [53]. Similarly, we could compare the difference in modular organization of the transportation network of different cities and relate their similarity or diversity in geometric separability of their modules to possible difference in transportation efficiency [54]. Through this study we applied a simplification that is to consider the community structure as a main example of mesoscale pattern in complex networks. This can be view as a limitation. For instance, other mesoscale structures such as echo chambers in social [55] and political [56] networks are an interesting phenomenon which could be investigated by applying geometric separability analysis. Investigating these research topics in future studies would not only demonstrate the versatility and adaptability of the proposed geometric separability analysis, but also its potential impact and utility in different real-world contexts. We hope that this discussion could motivate other scientists to bring forward research on geometric separability of mesoscale patterns in network science. This could significantly enhance the robustness of the findings presented in this study and underscore the broad applicability of the geometric separability measures to data emerging from various complex systems.

Methods

Data and algorithms

Synthetic data generation. In Fig 1, we generated an artificial network with 2 communities by using the nonuniform popularity similarity (nPSO) model[30,31] (available at https://github.com/biomedical-cybernetics/nPSO_model) with the following parameters' values: 30 as the total number of nodes, 4 as the half of average node degree, a temperature value of 0.1, a gamma value equal to 3, and 2 as the number of communities.

In Figs 5 and 6, we generated five small synthetic datasets with different shapes as a proof of concept to visualize and to inspect the differences between the linear and nonlinear separability measures described below. All datasets are composed of two main groups in a two-dimensional geometrical space.

Rhombus: It contains 20 samples (i.e., data points) arranged in a rhombus-like shape, with each group distributed on each side of the rhombus (i.e., each group is composed of 10 data points). Both groups have close proximity in the center of the shape.

Halfkernel: It contains 35 samples, but in this case, they are arranged in a halfkernel shape. The groups are separated by the two concentric semicircles, where the inner semicircle contains 15 data points, and the outer circle contains 20 data points.

Parallel lines: It contains 12 samples arranged as two parallel lines, each representing one of the two groups (i.e., each group is composed of 6 data points). The distance between the two lines is minimal; thus, the data points of the two different groups are very close to each other.

Circles: It is composed of 40 samples distributed as two concentric circles of different radius, each representing one of the two groups (i.e., each group is composed of 20 data points). The distance between the two circles is minimal; thus, the data points of the two different groups are very close to each other.

Spirals: It contains 55 samples distributed as two concentric spirals, each representing the two groups. The inner spiral contains 32 data points, whereas the outer spiral contains 23 data points. Both spirals have a common origin and separate as they get bigger.

These datasets are provided in the GitHub repository reported in the data availability section below.

Real complex multidimensional data. The radar signal dataset[42] was recovered from the UC Irvine Machine Learning Repository (available at http://archive.ics.uci.edu/ml/datasets/Ionosphere). It contains 350 valid radar signals targeting free electrons in the ionosphere. Shieh et al.[43] studied this dataset using two labeled groups (good and bad radar signals). However, they highlighted that good radar signals are highly similar and bad radar signals dissimilar. Later, Cannistraci et al.[32] confirmed that the bad radar signals can be interpreted as two diverse subcategories (two different groups) that are difficult to identify because of their high nonlinearity (elongated and irregular high-dimensional structure). Hence, in this study we consider the presence of three groups: good radar signal, bad radar signal type1 and bad radar signal type2.

Real complex networks. In this study, we considered eight real networks representing different social systems with mesoscale community structural organization. The networks have been transformed into undirected, unweighted, without self-loops, and only the largest connected component has been considered as in [31]. In addition, information about their ground truth communities is available.

The Zachary's Karate Club [57] (referred to as "Karate"), which contains 34 nodes and 78 edges. It represents the friendship between the members of a university karate club in the United States (US). It has two communities, formed by splitting the club into two parts, each representing a group of members following one trainer.

The American football network (referred to as "Football"), which contains 115 nodes and 613 edges, and represents the matches between Division IA of colleges in the fall of 2000 [18]. It is composed of twelve communities, which are the conferences each team belongs to.

The following networks (Opsahl 8, 9, 10, and 11) were downloaded from https://toreopsahl.com/datasets/. They represent an intra-organizational network described in[58]. Particularly, the networks Opsahl 8 and Opsahl 9 are the representation of a consulting company where the nodes represent employees. Opsahl 8 contains seven communities and has 43 nodes and 193 edges, indicating a link between employees who have at least turned to a co-worker for work-related information seldom. Similarly, Opsahl 9 contains seven communities, 44 nodes, and 348 edges; however, in this case, the links represent a relation between employees who consider the expertise of a co-worker important in the kind of work they do. On the other hand, Opsahl 10 and Opsahl 11 are networks that describe the interactions of a manufacturing company where the nodes represent employees. Opsahl 10 contains four communities, 77 nodes, and 518 edges, where the communities indicate the company locations (Paris, Frankfurt, Warsaw, and Geneva) where the employees were linked by which of their co-workers provided them - frequently or very frequently - with the information they used to accomplish their work. Similarly, Opsahl 11 contains the same number of communities and nodes but 1088 edges, where the employees were linked by their awareness of each other's knowledge.

Polblogs [59], which contains 1222 nodes and 16714 edges describing the links between blogs about politics in the 2004 US presidential election. It has two communities that represent the political tendencies of the blogs, such as conservative or liberal.

Polbooks (available at http://www-personal.umich.edu/~mejn/netdata/), which contains 105 nodes and 441 edges representing frequent co-purchases of books concerning US politics on *amazon.com*. It has three communities, each representing a political orientation, such as conservative, neutral, and liberal.

Network embedding methods. If we denote an undirected network as $G(V = \{1,\ldots,n\},E)$, i.e., as an abstract structure that is used to model a set E of relations (edges) over a set V of entities (nodes). Then, the main goal of network embedding is to find a mapping function $fV \mapsto R^d$ that projects each node into a d-dimensional space (where $d \ll |V|$) by preserving as much as possible the structural properties of the network (e.g., similar nodes in the network are embedded close together) [45,60,61]. With the aim of assessing if a network embedding provides a correct low-dimensional representation of a network, we used three state-of-the-art network embedding techniques, such as HOPE [34], ProNE [45], and Node2vec [46], whose resulting embeddings were quantitatively analyzed in terms of community separability by the approaches described in the next section to evaluate the extent to which these methods can correctly embed the networks in a low-dimensional space.

The first method, HOPE [34], is a matrix-factorization-based method, which preserves the high-order proximities of the networks and captures the symmetric transitivity of large-scale graphs. It has one hyperparameter to tune, defined as the "decaying constant", which determines how fast the weight of a path decays when the length of the path grows. We have set this parameter with its default value (0.5 divided by the spectral radius of the adjacency matrix), because according to some preliminary tests we found it does not substantially change the embedding in a way that is relevant for this study.

The second method, ProNE [45], is a network embedding method tailored for solving scalability issues in complex and large networks. It first formulates the network embedding as a sparse matrix factorization (SMF) to efficiently achieve the initial node representations, and secondly, it leverages the higher-order Cheeger's inequality to spectrally propagate the initial embeddings in a modulated network, capturing the network's localized and global clustering information. In this study, the outputs of the first step are referred to as ProNE (SMF), and the outputs of the second step are simply named ProNE. This method does not have extra hyperparameters to tune.

The third method, Node2vec [46], is a skip-gram-based approach, which returns feature representations that maximize the likelihood of preserving network neighborhoods of nodes in a reduced dimensional space by using a second-order random walk approach to generate (explore) different network's neighborhoods for nodes. This method provides control over the search space of neighborhoods for nodes by configuring two different hyperparameters: p which allows differentiating between inward and outward nodes by performing the search; and q which controls the likelihood of immediately revisiting a node during the walk while performing the search. We used all combinations of the values 0.5, 1.0, and 2.0 for p and q (i.e., nine different pairwise values), because according to some preliminary tests we noted they substantially change the embedding in a way that is relevant for this study.

Geometric separability indices. To quantitatively assess the extent to which the embedding of a method respects the intrinsic mesoscale structure of the data, we employed four indices to determine the community separability in the reduced geometrical space. Two indices were initially described by Acevedo et al [2] as projection separability indices (PSIs) tailored to assess linear separability. In this study, we refer to them as centroid projection separability (CPS) and linear discriminant projection separability (LDPS). One of the other two indices was originally proposed by Thornton[1], and is commonly known as the geometrical separability index (GSI), which is a measure able to assess nonlinear separability by computing the degree to which points associated with the same group cluster together. The last one, is a new

index proposed in this study to assess nonlinear separability based on the concept of the travelling salesman problem (TSP), which we called travelling salesman projection separability (TSPS). The three separability indices CPS, LDPS and TSPS were implemented adopting as discriminative measure the area under the precision-recall (AUPR) [16], which was employed to evaluate the level of discrimination of a pair of groups on the projection line or curve. We opted for the AUPR because it is robust when dealing with unbalanced groups [62,63]. Note that all these indices are bound between zero and one, where zero represents no separability and one perfect separability. In simple words, the closer to one the better the community separability.

Centroid projection separability (CPS) and linear discriminant projection separability (LDPS) indices. The linear separability indices CPS and LDPS quantify the community separability based on the projection separability (PS) rationale described in [2]. This means that the separability is assessed based on the pairwise comparisons of the groups (i.e., communities) present in the embedding.

In CPS, the separability evaluation of a pairwise group comparison is subject to the "centroid separability line"[2], which is calculated as follows: given two groups of samples (i.e., two different communities), the centroid of each group is computed (in this study, computed as the *median* of the positions of all points in a particular group); then, a line that connects both centroids is traced, and all points are projected onto this line (this is, the "centroid separability line").

In LDPS, this workflow is similar but differs on the underlying separability line, which in this case, is determined based on the first discriminant obtained by computing a linear discriminant analysis (LDA) of the two groups [2]. Thus, projecting the points onto this "discriminant line".

In both cases, the distance between a starting point (i.e., one of the line's extremes) to the rest of the points is calculated to generate a set of separability "scores." Finally, a statistical-based measure is applied to these scores to quantify the separability. In this study, this statistical-based measure is the area under the precision-recall curve (AUPR) [16], selected because of its robustness when dealing with unbalanced groups, which is the case of the studied networks.

If more than two communities are present, the procedure is repeated for all pairwise comparisons, and an overall separability estimation (in this case, the *mean* of all pairwise comparisons) is returned as the final separability value.

Geometrical separability index (GSI). The GSI [1] measures the degree to which inputs associated with the same output group together. In this case, this index computes the points' distances to all other points (in this study, the Euclidean distance) in the embedding. Then, it counts the matches when given a point, and its first neighbor shares the same group (in this case, a community) and divides this value by the total number of points. GSI quantifies to which extent the points of a group are geometrical separated from the ones in other groups. The upper-bound of GSI is one which means perfect separability.

Travelling salesman projection separability (TSPS). The TSPS is a measure we propose that is based on the solution of the travelling salesman problem, or TSP for short, which is one of the most intensively studied problems in computational mathematics [64]. TSP could be described as the problem of a salesman seeking the shortest tour through a N number of cities, passing by each city only once, and returning to the original starting point [65]. In other words, TSP can be described by a complete graph where the problem is to find a tour through its nodes of minimum total edge cost, where the tour must be a cycle that visits each node exactly once [40]. Despite this simple problem statement, solving the TSP is difficult since it belongs to the class of NP-complete problems [66]. Over the years, several methods to solve

TSP have been published. In this study, we used the best-known exact solver for provably optimal solutions of TSP called *Concorde* [40], available at https://www.math.uwaterloo.ca/tsp/concorde.html.

Concorde's algorithm implements a branch and bound strategy to search and generate solutions to TSP instances that are close to a global optimal. Based on this idea, we believe that Concorde can reveal a TSP tour that connects all nodes of a given low-dimensional embedding, which can be used as a nonlinear backbone for evaluating the community separability as follows: as in CPS and LDPS, we start by computing all pairwise group/community combinations. Then, we input a specific pairwise combination into Concorde to compute its TSP tour. Once the tour is generated, we remove the longest connection in the tour between nodes of different groups/communities to create a nonlinear path. We use this path to select a starting point (i.e., one of the path's extremes) and compute its distance to the rest of the points through the graph. This creates a set of separability scores which, as in CPS and LDPS, are used to compute the final separability value based on a statistical-based measure. In this case, we use the AUPR measure, as we also mentioned above, for CPS and LDPS. If more than two communities are present, the procedure is repeated for all pairwise group comparisons, and an overall estimator (in this case, the *mean*) is returned as the final separability value.

Statistical significance of the geometric separability measures. To evaluate the extent to which the results obtained by the truly-measured (observed) geometric separability measures/indices could be replicated at random, we used a statistical evaluation termed "trustworthiness" [2,67] that accounts for uncertainty, and associates to each separability index an empirical p-value that expresses the statistical significance of the index with respect to a null model. For a given embedding result, we evaluate the total number of pairwise combinations of the communities. In each pairwise comparison, we freeze the position of the underlying communities and reshuffle their group labels uniformly at random. We repeat this procedure 1000 times per pairwise combination (we selected this number because it offers an accurate estimation of the null model; however, it can be adapted concerning the user needs [2]), and the value of the evaluated index is recomputed in each round; thus, generating a random distribution of 1000 values on each pairwise combination. Then, we compute the mean over the pairwise combinations, obtaining 1000 results. Subsequently, we compute a p-value based on the number of values that surpassed the index's initial value (observed value). This p-value expresses the index's trustworthiness (separability significance) [2]. In this study, the p-values lower or equal to 0.01 are considered significant with respect to the null model distribution. Since our estimation is empirical, we decided to adopt the 0.01 threshold (instead of the more widespread 0.05) to be more conservative on the statistical estimation of significant deviation from randomness.

Adaptive assessment of the community separability. As previously described, we used two linear and two nonlinear separability indices. In certain scenarios, linear indices might fail in assessing nonlinear embedded structures where nonlinear indices can, and vice versa. Because of this, to obtain the best possible separability, our approach is to select the maximum results among the indices as an adaptive separability assessment and, at the same time, determine if the underlying separability type is linear or nonlinear. In this case, a linear separability is determined by CPS or LDPS, and a nonlinear separability is determined by GSI and TSPS. When the best separability is determined by both linear and nonlinear methods, then we select the separability type linear since nonlinear separability is exclusive.

Hardware and software

The software environments for executing the network embeddings and indices calculations were MATLAB 2021a and Python 3.6. These computations were executed at the ZIH of the TU Dresden, Intel Haswell, which has 612 nodes, each with 2 x Intel Xeon CPU E5-2680 v3 (12 cores) @ 2.50 GHz, Multithreading disabled, and 128 GB local memory on SSD.

The software environment for generating the images and tables was MATLAB 2022b. These computations were executed in a workstation under Windows 11 Home with 16 GB RAM and a processor Intel Core i7-8565U CPU @ 1.80GHz 1.99 GHz.

Acknowledgments

We thank: Massimiliano Di Ventra from UC San Diego for advice; Michael Schroeder, Björn Andres and Matthias Wählisch from TU Dresden for their comments; the Center for Information Services and High-Performance Computing (ZIH) of the TU Dresden and ScaDS.AI for providing HPC resources; the BIOTEC System Administrators for their IT support; Sabine Zeissig for the administrative assistance at BIOTEC; Yue Wu, Yuchi Liu, Qianyi Shao, Lixia Huang, and Weijie Guan for the administrative support at THBI; Hao Pang for the IT support at THBI.

Author Contributions

Conceptualization: Aldo Acevedo, Fabio Lorenzo Traversa, Carlo Vittorio Cannistraci.

Data curation: Aldo Acevedo, Yue Wu.

Formal analysis: Aldo Acevedo, Yue Wu.

Funding acquisition: Carlo Vittorio Cannistraci.

Investigation: Aldo Acevedo, Carlo Vittorio Cannistraci.

Methodology: Aldo Acevedo, Fabio Lorenzo Traversa, Carlo Vittorio Cannistraci.

Project administration: Carlo Vittorio Cannistraci.

Resources: Carlo Vittorio Cannistraci.

Supervision: Carlo Vittorio Cannistraci.

Validation: Aldo Acevedo, Yue Wu, Carlo Vittorio Cannistraci.

Visualization: Aldo Acevedo, Yue Wu, Carlo Vittorio Cannistraci.

Writing – original draft: Carlo Vittorio Cannistraci.

Writing – review & editing: Aldo Acevedo, Yue Wu, Fabio Lorenzo Traversa.

References

1. Thornton C. Separability is a learner's best friend. In: Bullinaria JA, Glasspool DW, Houghton G, editors. 4th Neural Computation and Psychology Workshop, London, 9–11 April 1997. London: Springer London; 1998. pp. 40–46.
2. Acevedo A, Duran C, Kuo M-J, Ciucci S, Schroeder M, Cannistraci CV. Measuring group separability in geometrical space for evaluation of pattern recognition and dimension reduction algorithms. IEEE Access. 2022; 10: 22441–22471. https://doi.org/10.1109/access.2022.3152789
3. Dunn JC. A fuzzy relative of the ISODATA process and its use in detecting compact well-separated clusters. Journal of Cybernetics. 1973; 3. https://doi.org/10.1080/01969727308546046
4. Calinski T, Harabasz J. A dendrite method for cluster analysis. Commun Stat Simul Comput. 1974; 3. https://doi.org/10.1080/03610917408548446

5. Davies DL, Bouldin DW. A cluster separation measure. IEEE Trans Pattern Anal Mach Intell. 1979; PAMI-1. https://doi.org/10.1109/TPAMI.1979.4766909 PMID: 21868852
6. Rousseeuw PJ. Silhouettes: A graphical aid to the interpretation and validation of cluster analysis. J Comput Appl Math. 1987; 20. https://doi.org/10.1016/0377-0427(87)90125-7
7. Bezdek JC, Pal NR. Cluster validation with generalized Dunn's indices. Proceedings - 1995 2nd New Zealand International Two-Stream Conference on Artificial Neural Networks and Expert Systems, ANNES 1995. 1995. https://doi.org/10.1109/ANNES.1995.499469
8. Hu L, Zhong C. An internal validity index based on density-involved distance. IEEE Access. 2019; 7. https://doi.org/10.1109/ACCESS.2019.2906949
9. Minsky ML, Papert S. Perceptrons - an introduction to computational geometry. expanded edition. MIT Press. 1969.
10. Minsky ML, Papert S. Perceptrons - an introduction to computational geometry: Epilogue. Handbook of attachment: theory, research, and clinical. MIT Press; 1988.
11. Fisher RA. The use of multiple measurements in taxonomic problems. Ann Eugen. 1936; 7. https://doi.org/10.1111/j.1469-1809.1936.tb02137.x
12. Cortes C, Vapnik V. Support-vector networks. Mach Learn. 1995; 20. https://doi.org/10.1023/A:1022627411411
13. Noble WS. What is a support vector machine? Nature Biotechnology. 2006. https://doi.org/10.1038/nbt1206-1565 PMID: 17160063
14. Abdiansah A, Wardoyo R. Time complexity analysis of support vector machines (SVM) in LibSVM. Int J Comput Appl. 2015; 128. https://doi.org/10.5120/ijca2015906480
15. Tsang IW, Kwok JT, Cheung PM. Core vector machines: Fast SVM training on very large data sets. Journal of Machine Learning Research. 2005; 6.
16. Raghavan V, Bollmann P, Jung GS. A critical investigation of recall and precision as measures of retrieval system performance. ACM Trans Inf Syst. 1989; 7: 205–229. https://doi.org/10.1145/65943.65945
17. Zhao Y, Zhang S, Xu J, Yu Y, Peng G, Cannistraci CV, et al. Spatial reconstruction of oligo and single cells by de novo coalescent embedding of transcriptomic networks. Adv Sci (Weinh). 2023/06/15. 2023; 10: e2206307–e2206307. https://doi.org/10.1002/advs.202206307 PMID: 37323105
18. Girvan M, Newman MEJ. Community structure in social and biological networks. Proc Natl Acad Sci U S A. 2002; 99: 7821–7826. https://doi.org/10.1073/pnas.122653799 PMID: 12060727
19. Darlington PJ. Carabidae of mountains and islands: data on the evolution of isolated faunas, and on atrophy of wings. Ecol Monogr. 1943; 13. https://doi.org/10.2307/1943589
20. Patterson BD, Atmar W. Nested subsets and the structure of insular mammalian faunas and archipelagos. Biological Journal of the Linnean Society. 1986; 28. https://doi.org/10.1111/j.1095-8312.1986.tb01749.x
21. Jonhson S, Domínguez-García V, Muñoz MA. Factors determining nestedness in complex networks. PLoS One. 2013; 8. https://doi.org/10.1371/journal.pone.0074025 PMID: 24069264
22. Borgatti SP, Everett MG. Models of core/periphery structures. Soc Networks. 2000; 21. https://doi.org/10.1016/S0378-8733(99)00019-2
23. Csermely P, London A, Wu L-Y, Uzzi B. Structure and dynamics of core/periphery networks. J Complex Netw. 2013; 1. https://doi.org/10.1093/comnet/cnt016
24. Gallagher RJ, Young JG, Welles BF. A clarified typology of core-periphery structure in networks. Sci Adv. 2021; 7. https://doi.org/10.1126/sciadv.abc9800 PMID: 33731343
25. Barzon G, Artime O, Suweis S, Domenico M De. Unraveling the mesoscale organization induced by network-driven processes. Proceedings of the National Academy of Sciences. 2024; 121: e2317608121. https://doi.org/10.1073/pnas.2317608121 PMID: 38968099
26. Zhang Yingtao, Zhao Jialin, Wu Wenjing, Muscoloni Alessandro, Cannistraci Carlo Vittorio. Epitopological learning and Cannistraci-Hebb network shape intelligence brain-Inspired theory for ultra-sparse advantage in deep learning. In: The Twelfth International Conference on Learning Representations (ICLR) 2024. 2024. pp. 1–29.
27. Cannistraci CV. Modelling self-organization in complex networks via a brain-inspired network automata theory improves link reliability in protein interactomes. Sci Rep. 2018; 8. https://doi.org/10.1038/s41598-018-33576-8 PMID: 30361555
28. Cavagna A, Cimarelli A, Giardina I, Parisi G, Santagati R, Stefanini F, et al. Scale-free correlations in starling flocks. Proc Natl Acad Sci U S A. 2010; 107. https://doi.org/10.1073/pnas.1005766107 PMID: 20547832

29. Vicsek T, Czirk A, Ben-Jacob E, Cohen I, Shochet O. Novel type of phase transition in a system of self-driven particles. Phys Rev Lett. 1995; 75. https://doi.org/10.1103/PhysRevLett.75.1226 PMID: 10060237

30. Muscoloni A, Cannistraci CV. A nonuniform popularity-similarity optimization (nPSO) model to efficiently generate realistic complex networks with communities. New J Phys. 2018; 20: 52002.

31. Muscoloni A, Cannistraci CV. Leveraging the nonuniform PSO network model as a benchmark for performance evaluation in community detection and link prediction. New J Phys. 2018; 20: 063022. https://doi.org/10.1088/1367-2630/aac6f9

32. Cannistraci CV, Alanis-Lobato G, Ravasi T. Minimum curvilinearity to enhance topological prediction of protein interactions by network embedding. Bioinformatics. 2013; 29: i199–i209. https://doi.org/10.1093/bioinformatics/btt208 PMID: 23812985

33. Kovács B, Palla G. Model-independent embedding of directed networks into Euclidean and hyperbolic spaces. Commun Phys. 2023; 6: 28. https://doi.org/10.1038/s42005-023-01143-x

34. Ou M, Cui P, Pei J, Zhang Z, Zhu W. Asymmetric transitivity preserving graph embedding. Proceedings of the ACM SIGKDD International Conference on Knowledge Discovery and Data Mining. New York, NY, USA: Association for Computing Machinery; 2016. pp. 1105–1114. https://doi.org/10.1145/2939672.2939751

35. Muscoloni A, Thomas JM, Ciucci S, Bianconi G, Cannistraci CV. Machine learning meets complex networks via coalescent embedding in the hyperbolic space. Nat Commun. 2017; 8: 1615. https://doi.org/10.1038/s41467-017-01825-5 PMID: 29151574

36. Zhang Y-J, Yang K-C, Radicchi F. Systematic comparison of graph embedding methods in practical tasks. Phys Rev E. 2021; 104: 44315. https://doi.org/10.1103/PhysRevE.104.044315 PMID: 34781460

37. Kojaku S, Radicchi F, Ahn Y-Y, Fortunato S. Network community detection via neural embeddings. 2023. https://doi.org/10.48550/arXiv.2306.13400

38. Tandon A, Albeshri A, Thayananthan V, Alhalabi W, Radicchi F, Fortunato S. Community detection in networks using graph embeddings. Phys Rev E. 2021; 103: 22316. https://doi.org/10.1103/PhysRevE.103.022316 PMID: 33736102

39. Cherifi H, Palla G, Szymanski BK, Lu X. On community structure in complex networks: challenges and opportunities. Appl Netw Sci. 2019; 4: 117. https://doi.org/10.1007/s41109-019-0238-9

40. Applegate DL, Bixby RE, Chvátal V, Cook W, Espinoza DG, Goycoolea M, et al. Certification of an optimal TSP tour through 85,900 cities. Operations Research Letters. 2009; 37: 11–15. https://doi.org/10.1016/j.orl.2008.09.006

41. Newman MEJ. Fast algorithm for detecting community structure in networks. Phys Rev E Stat Phys Plasmas Fluids Relat Interdiscip Topics. 2004; 69. https://doi.org/10.1103/PhysRevE.69.066133 PMID: 15244693

42. Sigillito VG, Wing SP, Hutton L V., Baker KB. Classification of radar returns from the ionosphere using neural networks. Johns Hopkins APL Tech Dig. 1989; 10: 262–266.

43. Shieh AD, Hashimoto TB, Airoldi EM. Tree preserving embedding. Proc Natl Acad Sci U S A. 2011; 108. https://doi.org/10.1073/pnas.1018393108 PMID: 21949369

44. Van Der Maaten LJP, Hinton GE. Visualizing high-dimensional data using t-sne. Journal of Machine Learning Research. 2008.

45. Zhang J, Dong Y, Wang Y, Tang J, Ding M. ProNE: fast and scalable network representation learning. Proceedings of the 28th International Joint Conference on Artificial Intelligence. 2019. pp. 4278–4284.

46. Grover A, Leskovec J. Node2vec: Scalable feature learning for networks. Proceedings of the ACM SIGKDD International Conference on Knowledge Discovery and Data Mining. New York, NY, USA: Association for Computing Machinery; 2016. pp. 855–864. https://doi.org/10.1145/2939672.2939754 27853626

47. Cannistraci CV, Muscoloni A. Geometrical congruence, greedy navigability and myopic transfer in complex networks and brain connectomes. Nat Commun. 2022; 13: 7308. https://doi.org/10.1038/s41467-022-34634-6 PMID: 36437254

48. Muscoloni A, Cannistraci CV. Minimum curvilinear automata with similarity attachment for network embedding and link prediction in the hyperbolic space. arXiv:180201183 [physics.soc-ph]. 2018.

49. Cai H, Zheng VW, Chang KC-C. A comprehensive survey of graph embedding: problems, techniques, and applications. IEEE Trans Knowl Data Eng. 2018; 30: 1616–1637. https://doi.org/10.1109/tkde.2018.2807452

50. Goyal P, Ferrara E. Graph embedding techniques, applications, and performance: a survey. Knowl Based Syst. 2018; 151: 78–94. https://doi.org/10.1016/j.knosys.2018.03.022

51. Cacciola A, Muscoloni A, Narula V, Calamuneri A, Nigro S, Mayer EA, et al. Coalescent embedding in the hyperbolic space unsupervisedly discloses the hidden geometry of the brain. 2017. Available: https://arxiv.org/abs/1705.04192
52. Zheng M, Allard A, Hagmann P, Alemán-Gómez Y, Ángeles Serrano M. Geometric renormalization unravels self-similarity of the multiscale human connectome. Proc Natl Acad Sci U S A. 2020; 117. https://doi.org/10.1073/pnas.1922248117 PMID: 32759211
53. Russell M, Aqil A, Saitou M, Gokcumen O, Masuda N. Gene communities in co-expression networks across different tissues. PLoS Comput Biol. 2023; 19. https://doi.org/10.1371/journal.pcbi.1011616 PMID: 37976327
54. Chen R, Lin Y, Yan H, Liu J, Liu Y, Li Y. Scaling law of real traffic jams under varying travel demand. EPJ Data Sci. 2024; 13: 30. https://doi.org/10.1140/epjds/s13688-024-00471-4
55. Wang X, Sirianni AD, Tang S, Zheng Z, Fu F. Public discourse and social network echo chambers driven by socio-cognitive biases. Phys Rev X. 2020; 10. https://doi.org/10.1103/PhysRevX.10.041042
56. Evans T, Fu F. Opinion formation on dynamic networks: Identifying conditions for the emergence of partisan echo chambers. R Soc Open Sci. 2018; 5. https://doi.org/10.1098/rsos.181122 PMID: 30473855
57. Zachary WW. An information flow model for conflict and fission in small groups. J Anthropol Res. 1977; 33: 452–473. https://doi.org/10.1086/jar.33.4.3629752
58. Cross R, Parker A. The hidden power of social networks: understanding how work really gets done in organizations. Harvard Business Publishing; 2004. https://doi.org/10.5860/choice.42-0398
59. Adamic LA, Glance N. The political blogosphere and the 2004 U.S. Election: Divided they blog. 3rd International Workshop on Link Discovery, LinkKDD 2005 - in conjunction with 10th ACM SIGKDD International Conference on Knowledge Discovery and Data Mining. New York, New York, USA: Association for Computing Machinery, Inc; 2005. pp. 36–43. doi: 10.1145/1134271.1134277
60. Yan S, Xu D, Zhang B, Zhang HJ. Graph embedding: A general framework for dimensionality reduction. Proceedings - 2005 IEEE Computer Society Conference on Computer Vision and Pattern Recognition, CVPR 2005. IEEE; 2005. pp. 830–837. https://doi.org/10.1109/CVPR.2005.170
61. Harel D, Koren Y. Graph drawing by high-dimensional embedding. Lecture Notes in Computer Science (including subseries Lecture Notes in Artificial Intelligence and Lecture Notes in Bioinformatics). Springer Verlag; 2002. pp. 207–219. https://doi.org/10.1007/3-540-36151-0_20
62. Fu GH, Xu F, Zhang BY, Yi LZ. Stable variable selection of class-imbalanced data with precision-recall criterion. Chemometrics and Intelligent Laboratory Systems. 2017; 171: 241–250. https://doi.org/10.1016/j.chemolab.2017.10.015
63. Ge Y, Rosendahl P, Duran C, Topfner N, Ciucci S, Guck J, et al. Cell mechanics based computational classification of red blood cells via machine intelligence applied to morpho-rheological markers. IEEE/ACM Trans Comput Biol Bioinform. 2021; 18: 1405–1415. https://doi.org/10.1109/TCBB.2019.2945762 PMID: 31670675
64. Applegate DL, Bixby RE, Chvátal V, Cook WJ. The traveling salesman problem: a computational study. Princeton University Press. 2011. https://doi.org/10.5860/CHOICE.45-0928
65. Laporte G. The traveling salesman problem: an overview of exact and approximate algorithms. Eur J Oper Res. 1992; 59: 231–247. https://doi.org/10.1016/0377-2217(92)90138-y
66. Hahsler M, Hornik K. TSP- infrastructure for the traveling salesperson problem. J Stat Softw. 2007; 23. https://doi.org/10.18637/jss.v023.i02
67. Durán C, Ciucci S, Palladini A, Ijaz UZ, Zippo AG, Sterbini FP, et al. Nonlinear machine learning pattern recognition and bacteria-metabolite multilayer network analysis of perturbed gastric microbiome. Nat Commun. 2021; 12: 1926. https://doi.org/10.1038/s41467-021-22135-x PMID: 33771992